Investigation of the effect mutations of CaM have upon *in vitro* and *ex vivo* function

by

Odisho K. Israel

A thesis

presented to the University of Waterloo

in fulfillment of the

thesis requirement of the degree of

Master of Science

in

Chemistry

Waterloo, Ontario, Canada, 2010

Author's declaration

I hereby declare that I am the sole author of this thesis. This is a true copy of this thesis, including any required final revisions, as accepted my by examiners.

I understand that my thesis may be made electronically available to the public.

Odisho K. Israel

Abstract

Calmodulin (CaM) is a calcium-binding protein that has promiscuous regulatory interactions with over three hundred intracellular protein targets. The focus of this study was to characterize the functional role of phosphorylated CaM *in vitro* and calcium-deficient CaM (Apo-CaM) *ex vivo*. In the *in vitro* study, the effect of phosphorylated CaM on the binding and activation of CaM target proteins was analyzed using mammalian Nitric Oxide Synthase (NOS). NOS is an enzyme that catalyzes the conversion of L-arginine to L-citrulline and •NO. In addition, the activation of NOS by modified CaM proteins was also analyzed in the presence of a CaM binding peptide, PEP-19.

Protein trafficking experiments were performed *ex vivo* to extend our understanding of Apo-CaM's functional role in mammalian cells. The cell lines that were used in this investigation include mouse Embryonic Stem Cells (mESC), Human Umbilical Vein Endothelia Cells (HUVEC) and Human Neuronal Glioma Cells (HNGC).

The major finding of this projects are: phosphorylation of selective CaM residues can attenuated NOS activity, electrostatic interactions are important in the activation of iNOS by CaM, and the activation of iNOS by CaM occurs in a calcium-dependent manner

Acknowledgements

I would like to thank my supervisor, Dr. Guillemette, for his guidance and support throughout the course of my graduate studies at the University of Waterloo.

I would like to thank my colleagues and friends from the Department of Chemistry for their support and good times. I would like to give a special thanks to Dr. Donald Spratt for being an excellent mentor when I first joined the lab.

I am grateful to have a wonderful graduate committee, Dr. Palmer and Dr. Meiring. Thank you for reading my thesis in a short period of time and for all the helpful advice you offered with respect to my project.

Finally, I want to thank my family for their love and support.

Dedication

To my little brother, ***Joe Israel***

Table of Contents

List of Figures

List of Tables

List of Abbreviation

AD	Autoinhibitory domain
Ahx	Aminohexanouic acid
Apo-CaM	Calcium-deficient CaM
BH_4	(6R)-5,6,7,8-tetrahydrobiopterin
Ca^{2+}	Calcium Ions
Camstatin	PEP-19 CaM binding peptide
CaM	Calmodulin
CK-II	Casein kinase 2
CPP	Cell Penetrating Peptide
LCM	Laser Confocal Microscopy
cNOS	Constitutive NOS (eNOS and nNOS)
CaM_{12}	CaM mutant incapable of binding to Ca^{2+} in its N-terminal EF-hand pairs
CaM_{34}	CaM mutant incapable of binding to Ca^{2+} in its C-terminal EF-hand pairs
CaM_{1234}	CaM mutant incapable of binding to Ca^{2+} in its N- and C-terminal EF-hand pairs
eNOS	Endothelial NOS
EGFRc-SRC	Epidermal growth factor receptor tyrosine kinase
FAD	Flavin-adenine dinucleotide
FMN	Flavin mononucleotide
FITC-TAT	FITC labeled TAT
FITC	Fluorescein isothiocyanate
HbO_4	Oxyhemoglobin assay
Heme	Iron Protoporphyrin IX
HFNC	Human Fetal Neuronal Cells
HNGC	Human Neuronal Glioma Cells
HUVEC	Human Umbilical Vein Endothelia Cells
InsR	Insulin Receptor
iNOS	Inducible NOS
mESC	Mouse Embryonic Stem Cells
MLCK	Myosin Light Chain Kinase
NADPH	Reduce nicotanamide adenine dinucleotide
NLS	Nuclear Localization Site
NGF	Nerve growth factor
NOS	Nitric Oxide Synthase
·NO	Nitric oxide
nNOS	Neuronal NOS
PTK-III	Protein Tyrosine Kinase III
TAT	Transactivator of Transcription
Texas Red	Rhoadamine Dye
TRITC	Tetramethyl Rhodamine Iso-Thiocyanate

Chapter 1

Literature review

This section briefly covers the background information on the proteins, enzymes and peptides that were used in this thesis. The following are subjects covered in this introduction: Calmodulin (CaM), PEP-19, Nitric Oxide Synthase (NOS) isozymes and Cell Penetrating Peptides (CPP).

1.1 Calmodulin

1.1.1 Calmodulin

CaM is a calcium sensing protein that plays an important role in important cellular processes such as apoptosis, cell proliferation, signal transduction, and gene transcription (Persechini *et al.*, 1991; Ikura *et al*., 2006). Three hundred intracellular CaM-binding proteins have been identified including Myosin Light Chain Kinase (MLCK), ion transporters such as Inositol triphosphate (IP_3), and NOS. In addition, CaM is the fifth most conserved mammalian protein (Ikura *et al.,* 2006).

As a result of the numerous target proteins and cellular pathways associated with CaM, a complete understanding of its functional role in the cell remains to be established. The numerous interaction of CaM makes it an appealing protein to investigate as one wonders how a single protein can selectively bind and/or activate so many proteins and cellular process simultaneously and discriminately.

1.1.2 Structural features of CaM

CaM is often described as a dumb-bell shaped structure connected by a central linker region (Yap *et al.*, 2000). The conformation of CaM changes upon calcium induction; it exhibits an extended conformation in its Holo-form and a compact conformation in its Apo-form as shown in Figure 1.1.

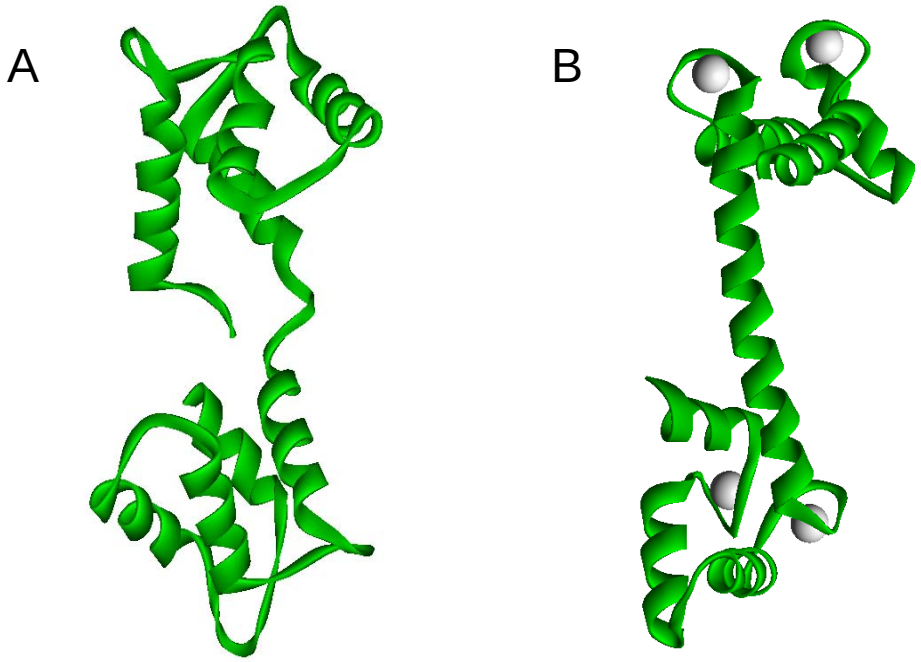

Figure 1.1 - Crystal (A) and NMR (B) structures of CaM. **(A)** Apo-CaM (Kuboniwa *et al.*, 1995) PDB 1CFD, **(B)** Holo-CaM (Chattopadhyaya *et al.*, 1992) PDB 1CLL. The white spheres represent calcium ions. The structural models were generated using ViewerLite 5.0 (Accelrys).

The structural plasticity of CaM is supported by the existence of nine methionine residues and the presence of a flexible central linker. Typically, 1% of a protein's amino acid residues are methionine; however, 6% of CaM's amino acid residues are methionine. These methionine residues are predominantly localized in the N-terminal and C-terminal domain of CaM. In

addition to methionine residues, the central linker helix enhances CaM's flexible nature by permitting the orientation of its two terminal domains to change independently. Therefore, CaM is able to accommodate a variety of different amino acid side chains in the target proteins (Trp, Phe, Ile, Val), thus allowing it to engage in a multiplicity of protein-protein interaction (Ikura *et al.,* 2006; Spratt *et al.*, 2008).

1.1.3 Conformation of CaM when bound to a target protein

NMR, X-ray crystallography and fluorescence-based methods have been employed to acquire detailed information on CaM's structural dynamics and protein-protein interactions with its target proteins. Such techniques include fluorescence polarization and Fluorescence (Förster) Resonance Energy Transfer (FRET), which can be used to monitor molecular domain interactions, mobility, enzyme function and changes in the intramolecular or intermolecular distances (Johnson, 2006; Spratt *et al.*, 2006). Based on these studies, CaM has been shown to assume several different conformations when bound to target proteins such as the Myosin Light Chain Kinase (MLCK), K^+ ion channel and Oedema factor as shown in Figure 1.2 (Drum *et al.*, 2002).

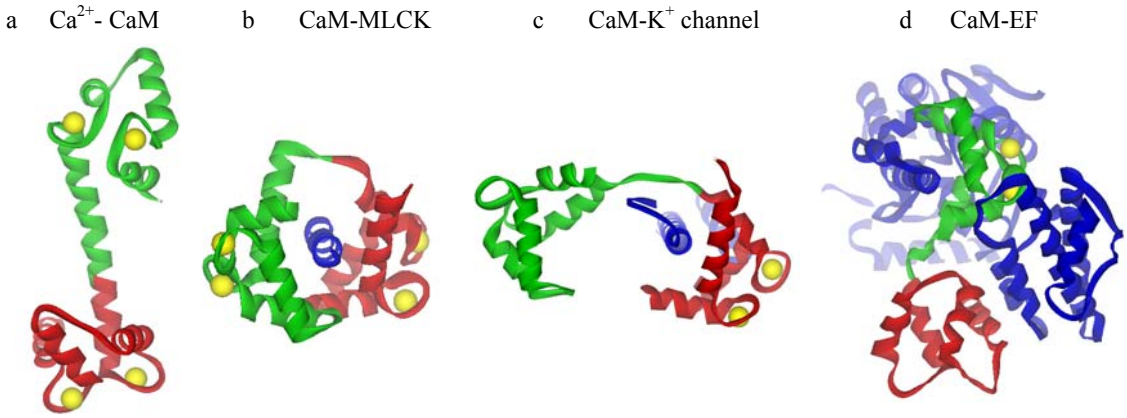

Figure 1.2 - Structural comparison of CaM binding conformations. Crystal representation of **a)** Ca^{2+}-CaM (PDB 1CLL) **b)** CaM in complex with the MLCK peptide **c)** CaM in complex with the Ca^{2+} - activated K^+ channel (PDB 1G4Y) and **d)** CaM in complex with the Oedema factor (PDB 1K93). The blue colored peptide is a representation of CaM-target peptide, while the green and the red colored protein regions represent CaM's C-terminal lobe and N-terminal lobe, respectively. The yellow colored spheres are calcium ions**.** Models were generated using ViewerLite 5.0 (Accelrys).

When bound to MLCK and the K^+ ion channel, CaM assumes a compact conformation with the hydrophobic facets of CaM lobes surrounding the amphipathic target helix (Drum *et al.*, 2002). Intriguing, however, is the conformation of CaM when in complex with the Oedema factor, whereby it adopts an abnormal binding conformation; instead of CaM acting like a clamp and surrounding the target protein, the Oedema factor surrounds and binds to CaM. Post-translational modification of CaM can to some degree modify its binding affinity to its target protein

1.1.4 Ca^{2+}- CaM

The majority of CaM's target proteins are activated in a calcium-dependent manner. CaM contains four calcium binding EF-hand motifs, equally divided between the N-terminal and C-terminal domains. The influx of calcium into the cytoplasm originates from either the extracellular space or from the intracellular reserves (rough endoplasmic reticulum). It has been

proposed that CaM, in its resting state, is bound to two Mg^{2+} ions within the N-terminal EF-hand pair, but the C-terminal EF-pair remains either metal free or calcium bound (Johnson, 2006). However, the Mg^{2+} ions are replaced with Ca^{2+} ions in response to elevated cytosolic Ca^{2+} concentrations (1-10 μM). In addition to Ca^{2+} ions, the activation of CaM-target proteins is also regulated by post-translational modifications of CaM itself (Gifford *et al.*, 2007).

1.1.5 Post-translational modification of Calmodulin

The interaction of CaM with certain target proteins can be regulated by modifying the CaM central linker region, residues 67-90. For instance, shortening the linker region can reduce the structural plasticity of CaM. In *ex vivo,* post-translation modifications of CaM, which include oxidation, acetylation, proteolytic cleavage, and phosphorylation, can serve as means of modulating CaM-target proteins, including NOS (Spratt *et al.*, 2008). However, the effects of such modifications of CaM on CaM-target proteins remain to be fully investigated. Protein phosphorylation is one of the most common processes employed by mammalian cells to regulate various enzymatic activities and cellular processes. There is great interest in investigating the functional role of phosphorylated CaM in the modulation of cellular processes, such as cell proliferation. Interestingly, of 18 amino acid residues in CaM that have been proposed as candidates for phosphorylation, only 8 have been verified to undergo this process by known kinases (Benaim *et al.,* 2002)(Figure 1.3).

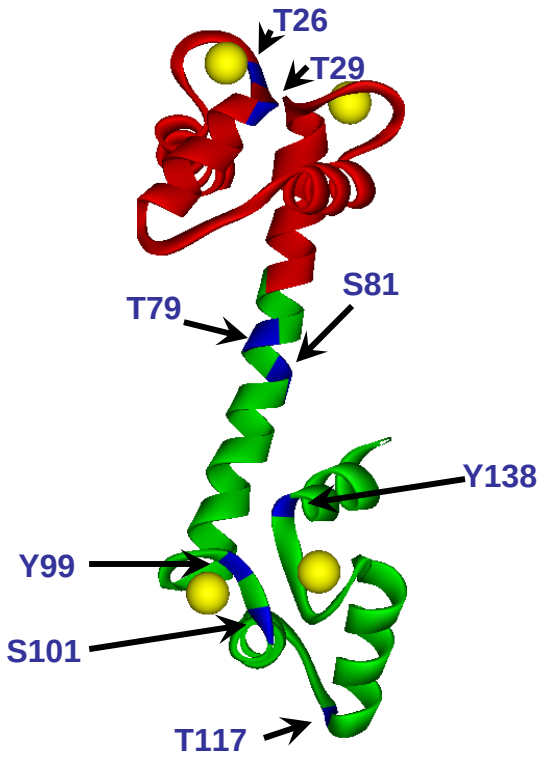

Figure 1.3 - Amino acid residues in CaM that have been shown to be phosphorylated *in vitro and ex vivo* (T79, S81, Y99 and S101). The blue regions are a representation of residues in CaM that can be phosphorylated by known kinases. The red and green regions represent the N- and C-terminal domains, respectively. Yellow spheres represent calcium ions. The model (PDB 1CLL) was generated using ViewerLite 5.0 (Accelrys).

The protein kinases that are known to phosphorylate CaM *in vitro are* listed in Table 1.1

(Benaim *et al.*, 2002).

Table 1.1 – Known phosphorylation sites in mammalian CaM.

Protein Kinase	Phosphorylated residues
Serine/threonine kinases	
CK-II	T79,S81,S101 (T117, *10%)
MLCK	T29 (T26, *10%)
Tyrosine kinases	
InsR	Y99 (Y138, *33%)
EGFRc-Src	Y99 (Y138, *15%)
PTK-III (c-Fyn + C-Fgr)	Y99 (Y138, *10%)
c-Src	Y99 (Y138, *26%)

* % of the residue in the parenthesis that was also phosphorylated by the same Kinase *in vitro.* This table is modified from Benaim *et al.* (2002).

1.2 IQ domains and PEP-19

PEP-19 protein, a member of small neuronal IQ motif proteins (SNIQP), is highly expressed in neuronal cells (~40 μM), particularly in Purkinje cells. This protein contains an acidic element and an IQ motif (IQXXXRXXXXX) that is recognized by Apo-CaM and Holo-CaM (Slemmon *et al.*, 1996). The IQ motif plays a key role in the binding of Pep-19 to CaM while the acidic element is essential in the modulation calcium binding to the C-domain of CaM (Putkey *et al.*, 2003; Dickerson *et al.*, 2006).

The binding of PEP-19 to Apo-CaM is 30 times slower than it is to Holo-CaM. In addition, the binding of PEP-19 to CaM results in a 40- to 50-fold increase in the rate of calcium association and dissociation to CaM by changing the conformation of CaM's C-domain. Such interaction is significant during signal transduction as the binding of calcium ions to CaM's C-terminal domain is too slow to respond to rapid transient calcium induction (Putkey *et al.*, 2003). For simplicity, PEP-19 derived peptide (residues 28-62; Figure 1.4) will be referred to as Camstatin, hereafter. It is important to note that Camstatin will mimic the function of PEP-19 (Putkey *et al.*, 2008).

Figure 1.4 – Amino acid sequence of Camstatin. The IQ motif is highlighted in blue and acidic element is exemplified by amino acid residues colored in red. The IQ motif is required for the binding of the peptide to CaM while the acidic element is needed for the modulation of calcium binding to CaM's C-domain.

The ability of Camstatin to bind to both Apo-CaM and Holo-form is of great interest. It has been proposed that Camstatin sequesters free intracellular CaM and prevents it from associating with other target-proteins (Kubota *et al.*, 2008). It has also been demonstrated that Camstatin can disrupt the activity of an enzyme in complex with CaM by directly associating with the enzyme's bound CaM (Dickerson *et al.*, 2006). Unlike other known neuronal CaM binding proteins that contain an IQ motif (such as neurogranin and neuromodulin), it is not known whether Camstatin is actually phosphorylated within the IQ domain as a regulatory step (Kubota *et al.*, 2008). However, it has been determined that phosphorylation of PEP-19 on a serine residue outside of the IQ domain by serine/threonine kinase does indeed occur *in vitro* (Dickerson *et al.*, 2006). In contrast to neuromodulin and neurogranin, such phosphorylation increases the affinity of Camstatin to CaM.

With respect to NOS isozymes, PEP-19, at a 30-fold higher molar concentration to CaM, attenuates CaM-dependent nNOS activity (Slemmon, 1996). This may be physiologically relevant because, as stated before, the concentration of PEP-19 in certain neuronal cells is up to 40-fold higher than that of CaM. Therefore, one of the objectives of this research project was to investigate NOS activation by CaM in the presence of Camstatin.

1.3 Nitric Oxide Synthase

Nitric Oxide (•NO) plays an important role in blood vessel dilation, neurotransmission and immune response (Alderton *et al.*, 2001). •NO is produced by Nitric Oxide Synthase (NOS), an enzyme that converts L-arginine and O_2 into L-citrulline and •NO by way of two successive mono-oxygenation reactions (Spratt *et al.*, 2006).

In mammals, NOS enzymes exist as one of three different isoforms including neuronal NOS (nNOS), endothelial NOS (eNOS), and inducible NOS (iNOS) (Yap *et al*., 2000; Spratt *et al*., 2006). These NOS isoforms differ in their expression and calcium dependence. While eNOS and nNOS are constitutively expressed and are Ca^{2+}-CaM dependent enzymes, iNOS is inducibly expressed and binds to CaM in a Ca^{2+}-independent manner (Spratt *et al.*, 2007b).

1.3.1 Structural features of NOS

NOS is active in its dimer form with each monomer bound to L-arginine and five cofactors: FAD, FMN, Heme, Tetrahydrobiopterin (H_4B), and NADPH (Johnson, 2006). Each monomer is composed of two functionally independent domains, an amino terminal oxygenase domain and a carboxy-terminal reductase domain, separated by a CaM binding motif (Figure 1.5)

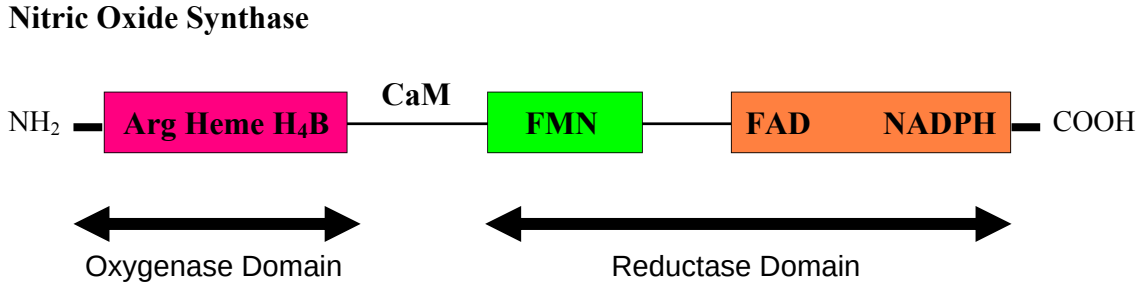

Figure 1.5 - A general schematic presentation of NOS domains and sub-domains. The CaM binding site is located between the oxygenase and reductase domains. This figure is modified from Aldeton *et al.* (2001).

The reductase domain contains a binding site for FAD, FMN, and NADPH cofactors, whereas heme, L-arginine, and H_4B are localized in the oxygenase domain (Alderton *et al.*, 2001). The electron flow between the two domains is initiated when CaM binds to the amphipathic linker region of NOS, thus allowing for the production of •NO and L-citrulline

(Alderton *et al.*, 2001; Spratt *et al.*, 2006). The actual mechanism by which electrons are transferred between the two domains has not been fully established, but it is believed that the binding of CaM results in a major structural rearrangement of NOS, specifically within the FMN domain. It has been suggested that the FMN domain is highly dynamic due to a hinge region, thus, the binding of CaM to NOS is followed by the structural rearrangement of the FMN domain, permitting the delivery of electrons to the oxygenase domain (Ghosh *et al.,* 2003). The electron transfer pathway in NOS commences in the reductase domain with the hydrogenation of NADPH. Subsequently, this process initiates a cascade of electron flow along the reductase domain involving the flavin cofactors and ending within the oxygenase domain. The transfer of electrons to the oxygenase domain is the rate liming step (Spratt *et al.*, 2007a). Depending on the NOS isoform, this enzymatic process can be regulated in the cell by post-translational modifications (e.g. phosphorylation), heat shock protein 90, and by changes in the intracellular calcium concentration (Alderton *et al.*, 2001).

1.4 Cell penetrating peptides

The introduction of therapeutics and reporter molecules across the plasma membrane requires an efficient delivery method. Traditional delivery methods such as microinjection, electroporation, chemical transfection, viral delivery systems, and liposome encapsulation have been used to introduce various cargo molecules into the cell (Trehin *et al*., 2004; Wadia *et al.,* 2005). However, all of these methods are prone to low internalization efficiency and high cellular toxicity. To characterize the functional role of Apo-CaM and phosphorylated CaM in the cell, a cell penetrating peptide (CPP) was used as a vector to deliver CaM protein into the cell.

CPPs are short (<30 amino acid) basic peptides capable of cell membrane permeation (Trehin *et al*., 2004; Wadia *et al.,* 2005). Currents studies employ CPPs to introduce various cargo molecules into live mammalian cells. The cargo molecule, ranging from a nano particle to a protein, is generally coupled to the CPP by a covalent bond, such as a disulfide bond or a peptide bond (Fonseca *et al.*, 2009). Such cargo molecules include DNA, metal particles, antibodies and proteins (Wadia *et al.,* 2005). Over 10 different CPPs derived from either a synthetic or biological source are currently being used by research groups to study various cellular phenomena (Table 1.2). For example, clinical trials are underway for the treatment of Duchenne muscular dystrophy in the UK and the Netherlands. These research groups have introduced CPP attached phosphorodiamidate morpholino oligomer (~30-mer; CPP-PMO) by intramuscular injection in humans to target a mutated dystrophin exon, thereby restoring dystrophin to normal levels (Wu *et al.*, 2008; Said Hassane *et al.*, 2009). It is important to note that each CPP consists of a different translocation efficiency and cellular toxicity (Trehin *et al*., 2004; Wadia *et al.,* 2005).

Table 1.2 - A List of cell penetrating peptides (Said Hassane *et al.*, 2009)

Cell penetrating peptide	**Amino acid sequence**
Tat	RKKRRQRRR
Polyarginines	RRRRRRRRR
Penetratin	QQIKIWFQNRRMKWK
Decalysine	KKKKKKKKKK
POD	$GGG(ARKKAAKA)_4$

In this thesis, a CPP derived from Transactivator of Transcription protein (Tat peptide; see Table 1.2) of HIV-1 virus was chosen as a vector to introduce cargo molecules across the cell membrane due to its very high translocation efficiency and low cellular toxicity (Sugita *et al*, 2008). The physiological effects and protein trafficking of Apo-CaM, excess wild-type CaM and CaM mutant proteins in the cell will be monitored by fluorescence microscopy.

1.4.1 Transactivator of transcription peptide

Transactivator of Transcription peptide (TAT) is a cell penetrating peptide derived from HIV-1 transactivator of transcription protein. TAT, an 11 amino acid basic peptide is composed of mainly arginine and lysine residues (YGRRKKRQRRR). The peptide itself contains two functional elements separated by a linker region (RQ). Each element has its own function; the N-terminal element (YGRRKK) is essential for nuclear localization of the peptide, while the C-terminal element (RRR) plays a pivotal role in the internalization of the peptide into the cell. Mutation or removal of any arginine residues in the peptide will reduce the internalization efficiency by 50% (Efthymiadis *et al.*, 1998). The cargo-translocation delivery process employed by this peptide is yet to be determined as published data are plagued with artifacts. However, it has been hypothesized that TAT peptide permeates the cell membrane by one of the following delivery system: endocytosis, micelle-driven delivery, or by direct penetration of the plasma membrane (Trehin *et al.,* 2004) (Figure 1.6).

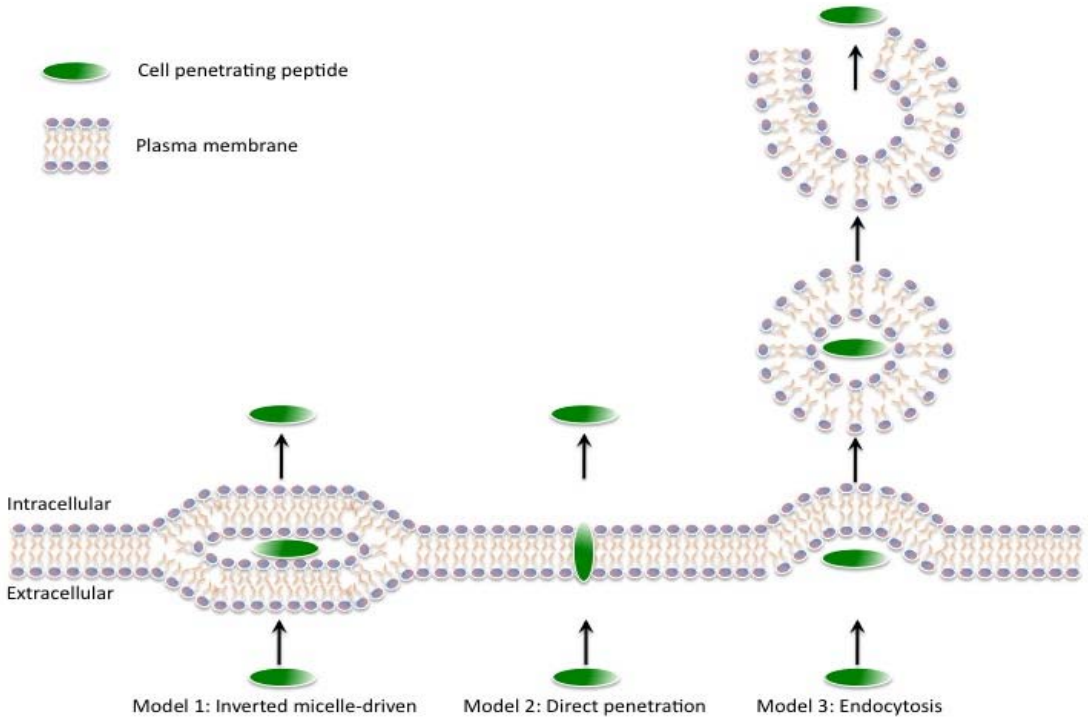

Figure 1.6- Proposed mechanisms of cargo delivery utilized by TAT peptide.
Models 1 and 2 are reported to occur through an energy-receptor independent process, whereas model 3 occurs through an energy–receptor dependent process.

The exact mechanism for cellular internalization of TAT peptide remains controversial. However, it has been suggested that the first step in the internalization process involves an electrostatic interaction between the positively charged residues of TAT and the negatively charged membrane constituents, such as proteoglycans, heparin and clathrin coated pits (Trehin *et al.,* 2004; Tilstra *et al.*, 2007). The subsequent step is the uptake of the cargo molecule by endocytosis or direct penetration of the cell membrane. Unfortunately, according to current literature, the majority of cargo molecules become trapped in the late endosome, only to be degraded in the lysosome if shuttling to the nucleus or release into the cytoplasm fails. However, new methods have been developed to facilitate the release of trapped cargo molecules from

endosomes. For instance, the attachment of a poly-histadine tag on both sides of the TAT peptide will, to some extent, disrupt the endosomal membrane by dehydration to liberate trapped TAT from the endosome. The final destination of free TAT in the cell is the nucleus, where it will remain there for the duration of 24 hours before degraded. The method of utilizing CPPs to introduce cargo molecules into live cells can be applied for this *ex vivo* study to monitor the functional role of Apo and post-translationally modified CaM.

Chapter 2

Regulation of mammalian nitric oxide synthase by electrostatic interactions in the linker region of calmodulin*

2.1 Introduction

The promiscuity of CaM in its binding to numerous target proteins is due to the existence of a central linker region. The CaM central linker region acts as a flexible tether that permits variable orientation of the terminal domains in association with target proteins (Persechini *et al.*, 1988). The linker region can also undergo phosphorylation and other post-translational modifications within the cell (Benaim *et al.,* 2002). The role of the central linker region and electrostatic interaction of CaM in the binding and activation of target proteins have been investigated using truncated CaM, charge substituted CaM (negative to positive) and phosphomimetic CaM mutants. Deletion of a single residue in the central linker region of CaM brings the two terminal domains closer to each other by 1.5 Å and alters the orientation of the lobes by 100º relative to one another (Persechini *et al.*, 1989). Persechini *et al.* (1989) have reported changes in the activation profile of different CaM-target enzymes by central-linker truncated CaM mutants: CaM Δ 81-84, Δ83-84 and Δ84.

The kinetics assays for cNOS enzymes with mutant CaM were performed by Spratt. The kinetics assays for iNOS enzyme with mutant CaM were performed by Israel. Circular dichroism experiments were performed by Israel. Gel shift mobility assays were performed by Israel. CaM proteins were expressed and purified by Israel, Spratt and Taiakina.

CaM residue E82, E83 and E84 are all negatively charged amino acids, which plays a key role in the association of CaM with its target proteins. Although the effect truncated CaM proteins (CaM Δ 81-84, Δ 83-84, Δ 84) on nNOS activity was analyzed, the activation profile for eNOS and iNOS with these mutants was unknown prior to our investigation. Our aim was to determine if the inactivation of NOS isozymes by central linker truncated CaM mutants were a result of changes in the electrostatic interaction within the CaM-NOS complex. Furthermore, a set of mutations in the CaM central linker region was introduced, whereby glutamates (E84 and E87) were substituted with positively charged amino acid residues (arginine and lysine) to investigate the importance of electrostatic interaction between the CaM linker region and NOS

In addition, to study the role of phosphorylated CaM in the activation of NOS isozymes with respect to electrostatic interaction, phosphomimetic CaM mutants were generated. Phosphomimetic CaM mutants are modified CaM proteins with serine/threonine and tyrosine residues substituted with aspartic and glutamic acid, respectively (Figure 2.1.0).

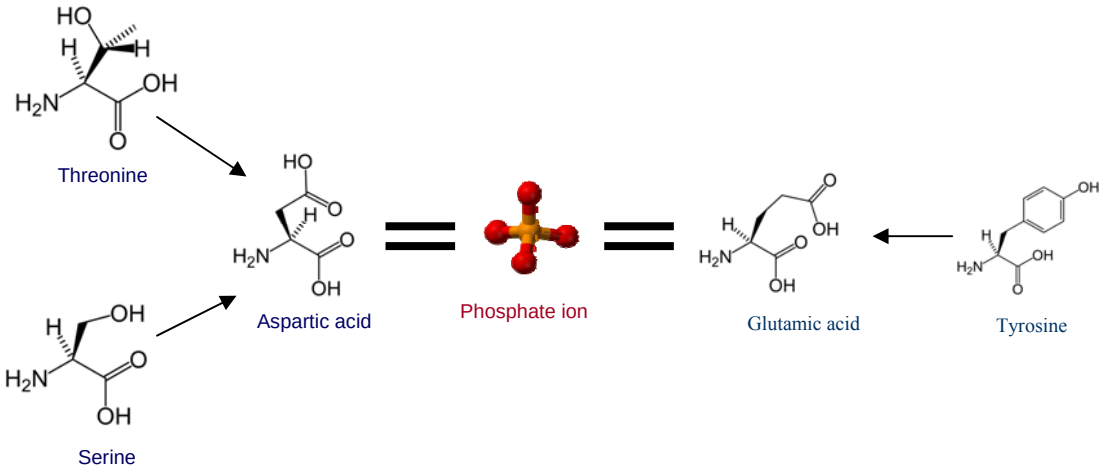

Figure 2.1.0- Schematic diagram illustrating phosphomimetic amino acid residues. Threonine, serine and tyrosine are substituted with aspartic or glutamic acid to mimic a phosphate ion with respect to charge within a protein.

Aspartic and glutamic acid can imitate a phosphate ion in regards to the negative charge it possesses. Studies by (Greif *et al.*, 2004) have shown that phosphomimetic CaM proteins can mimic the functional role of phosphorylated CaM. In their study, phosphorylated CaM S101 attenuated eNOS activity by ~30% (Greif *et al.*, 2004). However, the change in eNOS activity by phosphorylated CaM S101 was not addressed nor did the authors propose a mechanism to explain such attenuation. In contrast to attenuation of eNOS by phosphorylated CaM S101, the Carafoli group reported a 2.6-fold increase in nNOS activity by phosphorylated CaM catalyzed by Casein kinase 2 (CK-II) (Quadroni *et al.*, 1998). Casein kinase 2 simultaneously targets CaM T79, CaM S81, and CaM S101 for phosphorylation (Quadroni *et al.*, 1994). However, it was not determined which of these residues played a key role in the up-regulation of nNOS activity. Although extensive studies on eNOS activation by phosphorylated CaM have been published, the iNOS activation profile by phosphorylated CaM was unknown until now.

In summary, a series of central linker CaM mutants was generated to investigate the importance of electrostatic interaction in the binding and activation of Ca^{2+}- independent iNOS enzyme and Ca^{2+}-dependent cNOS enzymes.

2.2 Experimental procedures

2.2.1 Mutations of CaM

Vectors coding for phosphomimetic CaM mutants T79D, CaM S81D, CaM T79D/S81D, CaM S101D and CaM Δ84 in the kanamycin resistant pET9dCaM plasmid (Spratt *et al.*, 2006) were developed using The QuikChange site-directed mutagenesis procedure (Wang *et al.,* 1999). Vectors coding for truncated CaM mutants (Δ81-84, CaM Δ83-84, and Δ84 in pKK233-2) and charged CaM mutants (CaM E84R/E87K in pET23b) were generous gifts from Dr. John

Adelman (Oregon Health & Sciences University, Portland, OR, USA; (Lee *et al.*, 2003) and Dr. Anthony Persechini (University of Missouri at Kansas City, MI, USA; (Persechini *et al.*, 1989), respectively. PCR amplification was used to introduce *Nco*I and *Sac*I cut sites in the pET28a (Novagen) vectors of CaM E84R/E87K, CaM Δ81-84 and CaM Δ83-84 DNA constructs. The primers that were used in the PCR mutagenesis and cloning of these vectors (CaM E84R/E87K, CaM Δ81-84 and CaM Δ83-84) are summarized in Table 2.1.0.

Table 2.1.0- Primers used for CaM mutagenesis

CaM protein	Primer	
Mutagenesis		
CaM T79D	CaMT79Dfr	5' CTGACAATGATGGCGCGCAAAATGAAAGACGACGACAGTGAAGAAGAAATTAG 3'
	CaMT79Drv	5' CTAATTTCTTCTTCACTGTCGTCGTCTTTCATTTTGCGCGCCATCATTGTCAG 3'
CaM S81D	CaMS81Dfr	5' ATGAAAGACACAGACGATGAAGAAGAAATTCGCGAAGCGTTCCGTTCC 3'
	CaMS81Drv	5' GGAACGGAACGCTTCGCGAATTTCTTCTTCATCGTCTGTGTCTTTCAT 3'
CaM T79D/S81D	CaMTS2Dfr	5' GCAAGAAAAATGAAAGACGACGACGATGAAGAAGAAATTCGCGAAGCGTTCCGTTCC 3'
	CaMTS2Drv	5' GGAACGGAACGCTTCGCGAATTTCTTCTTCATCGTCGTCGTCTTTCATTTTTCTTGC 3'
CaM S101D	CaMS101Dfr	5' GCAATGGCTACATCGACGCAGCAGAGCTCCGCCACGTGATGAC 3'
	CaMS101Drv	5' GTCATCACGTGGCGGAGCTCTGCTGCGTCGATGTAGCCATTGC 3'
CaM Δ84	CaMΔ84fr	5' CACAGACAGTGAAGAAATTAGAGAGGCCTTCCGTGTGTTTGATAAG 3'
	CaMΔ84rv	5' CTTATCAAACACACGGAAGGCCTCTCTAATTTCTTCACTGTCTGTG 3'

2.2.2 CaM protein expression and purification

Wild-type CaM and mutant CaM proteins were expressed and purified using affinity chromatography (phenyl sepharose), as previously described (Spratt *et al*., 2006). The purity of the proteins was confirmed using ESI-MS and SDS-PAGE analysis, as described in Spratt *et al*. (2006).

2.2.3 Binding of CaM central linker mutant proteins to synthetic NOS peptides

Secondary structures of CaM in complex with NOS-CaM binding domains were analyzed using Circular Dichroism (CD). CD analysis was conducted with a Jasco J-715 CD spectropolarimeter, using J-715 analysis software as previously described (Spratt *et al.*, 2007b). Prepared samples consisted of 10 μM wild-type CaM or mutant CaM proteins alone or with equimolar concentrations of synthetic NOS CaM-binding domain peptide. The NOS CaM-binding domain peptides for bovine eNOS (TRKKT FKEVA NAVKI SASLM; residues 493–512), rat nNOS (KRRAI GFKKL AEAVK FSAKL MGQ; residues 725–747), and human iNOS (RPKRR EIPLK VLVKA VLFAC MLMRK; residues 507–531) were synthesized by Sigma-Genosys (Oakville, ON, Canada). Samples were mixed in a buffer consisting of 10 mM Tris-HCl, pH 7.5, 150 mM NaCl, 200 μM $CaCl_2$, and 1 mM EDTA. Gel shift mobility assays were performed as previously described (Spratt *et al*., 2006).

2.2.4 NOS expression and purification

cNOS enzyme, rat nNOS and bovine eNOS were expressed as previously described (Roman *et al*., 1995; Martasek *et al.*, 1996) with the exception that these constructs had an N-terminal polyhistidine tail cloned upstream from their respective start codons. Human iNOS, carrying a deletion of the first 70 amino acids and an N-terminal polyhistidine tail, was co-expressed with wild-type CaM or mutant CaM protein in E. coli BL21 (DE3) (Newman *et al.*, 2004). Ammonium sulfate precipitation, metal chelation chromatography, and 2’5’-ADP sepharose chromatography were employed to purify the NOS enzymes. iNOS was co-expressed with CaM as previously described by Spratt (Spratt, 2008).

2.2.5 Enzyme kinetics

The enzyme kinetics tools that were used to measure and monitor the electron transfer rates in the NOS are NADPH oxidation, cytochrome c reduction, and the oxyhemoglobin capture assays (Figure 2.1), as previously described (Gachhui *et al*., 1996; Montgomery *et al*., 2000; Montgomery *et al*., 2003; Spratt *et al*., 2007a). Assays were performed in 96-well microtitre plates at 25 °C in a SpectraMax 384 Plus 96-well UV–visible spectrophotometer equipped with Soft Max Pro software (Molecular Devices, Sunnyvale, CA).

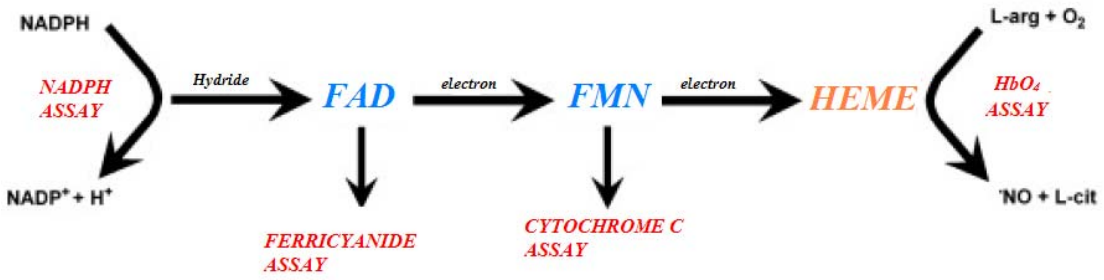

Figure 2.1.1-Spectroscopic assays (in red color) that can be used to monitor electron flow and ·NO production within NOS. The NADPH assay measures the oxidation of NADPH .The ferricyanide assay measures the hydride transfer to the FAD. The cytochrome c assay measures electron transfer through the reductase domain to the FMN. The oxyhemoglobin (HbO_4) capture assay measures the production of •NO from L-arginine. This figure was modified from (Spratt *et al.*, 2007a).

2.3 Results

2.3.1 Characterization of mutant CaM proteins

Purification of CaM resulted in over 95% homogeneity, as judged by SDS-PAGE analysis (Figure 2.2). ESI-MS confirmed the actual molecular weight of CaM mutants to be the same as the theoretical size (Table 2.1). Structural data for CaM mutants obtained via CD analysis revealed that it was identical to wild-type CaM (wtCaM) in the presence of Calcium

ions and EDTA, with respect to its alpha-helical content. CD analysis revealed no significant change in the alpha-helical content when compared to wtCaM in the presence of calcium for CaM mutants (truncated, charged and phosphomimetic mutants) in complex with the cNOS, eNOs and nNOS, CaM- binding peptide. However, there were significant changes in the secondary structure of iNOS peptide bound to CaM mutants in the presence of EDTA (CaM 81-84, CaM E84R/E87K), where a decrease in alpha-helical content was observed (Figure 2.3). Gel shift mobility analysis for all CaM mutants in complex with NOS-CaM binding domain peptides showed an association ratio of 1:1.

.

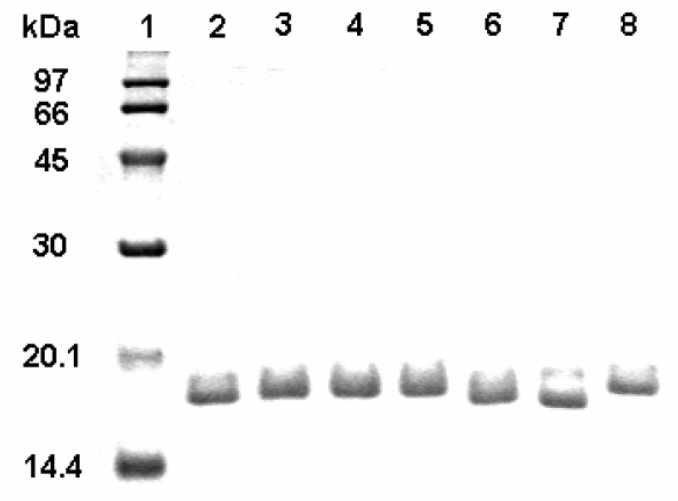

Figure 2.2 – 15% SDS-PAGE analysis of purified CaM proteins. A 10 μg sample of each purified CaM protein was loaded in a standard SDS-PAGE loading buffer containing 1 mM EDTA. Lane 1, low molecular mass protein standard (GE Healthcare); Lanes 2 & 8, wild-type CaM; Lane 3, CaM T79D; Lane 4, CaM S81D; Lane 5, CaM T79D/S81D; Lane 6, CaM S101D; Lane 7, CaM E84R/E87K.

Table 2.1.1 – Masses of phosphomimetic/charged and central linker deletion CaM proteins

	Mass (Da) [a]	
CaM proteins	Observed	Theoretical [b]
Wild-type CaM	16706.0	16706
Phosphomimetic /Charge CaMs		
CaM T79D	16718.5	16720
CaM S81D	16731.5	16734
CaM T79D/S81D	16746.5	16748
CaM S101D	16732.5	16734
CaM E84R/E87K	16730.5	16733
Central Linker Deletion CaMs		
CaM Δ84	16575.0	16577
CaM Δ83-84	16446.0	16448
CaM Δ81-84	16230.0	16232

[a] Masses of deconvoluted ESI-MS spectra were determined with an accuracy of ± 5 Da.

[b] Calculated masses based upon amino acid sequence.

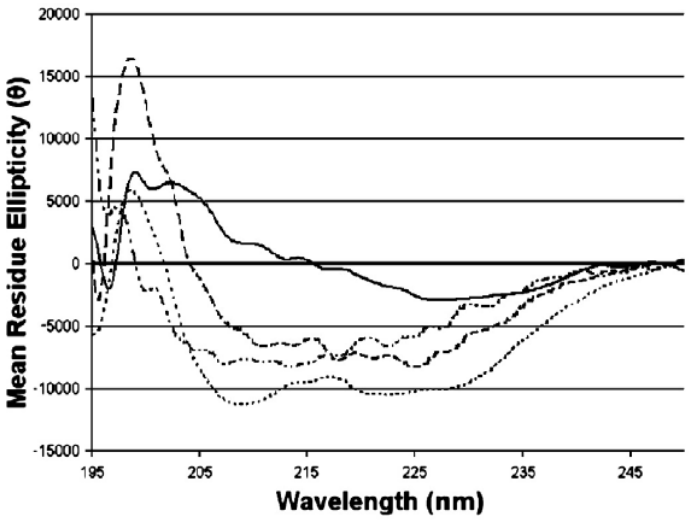

Figure 2.3 - Difference CD spectra for iNOS CaM binding domain peptides bound to wild-type CaM and mutant proteins. Difference spectra for the iNOS peptide were calculated by subtracting the spectra of 10 μM CaM in the presence of EDTA from the spectra of 10 μM CaM in the presence of 10 μM peptide and EDTA. Difference spectra are represented as shown in parenthesis: wild-type CaM (----), CaM Δ81-84 (— —), CaM E84R/E87K (—), and iNOS peptide (— - - —). Data are expressed as the mean residue ellipticity (Θ) in degree cm^2 $dmol^{-1}$

2.3.2 Effect of phosphomimetic and charge mutant CaM proteins on NOS activation

The rate of in •NO production measured from the oxyhemoglobin assay marked a decrease in iNOS catalytic activity of 10-20 % by phosphomimetic CaM (Table 2.2). The addition of excess EDTA in the presence of wtCaM and phosphomimetic CaM mutants (with exception to CaM E84R/E87K) resulted in slight reduction of iNOS activity, which is consistent with previous studies (Venema *et al*., 1996; Newman *et al*., 2004; Spratt *et al*., 2006; Spratt *et al*., 2007a). However, the activity of iNOS was significantly reduced by CaM E84R/E87K in comparison to wtCaM and phosphomimetic mutants. In addition, a Ca^{2+}-dependent activation of iNOS is observed in the presence of 250 μM EDTA (Table 2.2).

Table 2.2– Phosphomimetic/charged and central linker mutant CaM protein activation of iNOS [a]

CaM protein	NADPH oxidation		Cyt *c* reduction		•NO synthesis		
	200 μM $CaCl_2$ %	250 μM EDTA %	200 μM $CaCl_2$ %	250 μM EDTA %	200 μM $CaCl_2$ %	250 μM EDTA %	250 μM EDTA with 3 μM CaM %
CaM	100 ± 3	86 ± 4	100 ± 4	84 ± 5	100 ± 4	87 ± 2	82 ± 2
Phosphomimetic /Charge CaMs							
CaM T79D	106 ± 1	95 ± 2	120 ± 4	108 ± 5	82 ± 2	62 ± 3	74 ± 3
CaM S81D	104 ± 1	103 ± 3	169 ± 3	170 ± 5	91 ± 3	74 ± 3	77 ± 3
CaM T79D/S81D	102 ± 1	98 ± 3	149 ± 1	130 ± 2	90 ± 3	81 ± 3	84 ± 4
CaM S101D	103 ± 3	97 ± 3	153 ± 3	154 ± 2	88 ± 1	68 ± 1	75 ± 2
CaM E84R/E87K	101 ± 1	52 ± 1	133 ± 1	108 ± 3	71 ± 1	7 ± 1	50 ± 2
Central Linker Deletion CaMs							
CaM Δ84	110 ± 5	109 ± 5	160 ± 4	147 ± 3	64 ± 3	20 ± 1	48 ± 2
CaM Δ83-84	124 ± 4	120 ± 3	160 ± 3	154 ± 1	65 ± 3	9 ± 1	51 ± 2
CaM Δ81-84	116 ± 3	103 ± 3	134 ± 3	120 ± 2	67 ± 3	5 ± 1	50 ± 2

[a] •NO synthesis, cytochrome *c* reduction and NADPH oxidation rates were measured with no exogenous CaM added to the assay. Each assay was performed in the presence of either 200 μM $CaCl_2$ or 250 μM EDTA as indicated. The activities obtained for iNOS coexpressed with CaM and assayed in the presence of 200 μM $CaCl_2$ at 25°C were all set to 100% and were 50 min^{-1} (•NO synthesis), 82.4 min^{-1} (NADPH oxidation) and 1486 min^{-1} (cytochrome *c* reduction).

Both cytochrome c reduction rates and NADPH oxidation rates for iNOS co-expressed phosphomimetic CaM proteins were slightly higher in comparison to wild-type CaM in the presence of calcium ions. However, chelation of calcium ions resulted in a decreased of both cytochrome c reduction rates and NADPH oxidation rates for iNOS co-expressed with phosphomimetic CaM proteins (Table 2.2).

Unlike iNOS, the eNOS enzyme maintained a 100% activity when in complex with phosphomimetic CaM mutants, with exception to CaM S101D, a 20% decrease in eNOS enzyme activity is observed. In addition, charge CaM mutant protein reduced eNOS activity by 74%. Data extracted from NADPH oxidation and cytochrome *c* reduction assays presented a similar trend for eNOS activation with each CaM mutant.

A slight attenuation nNOS activity was observed by all phosphomimetic CaM proteins by a decrease in •NO production. This data is supported by previous studies where differences between eNOS and nNOS activation profiles, using a variety of CaM mutants, were observed (Montgomery *et al.*, 2003; Newman *et al.*, 2004; Spratt *et al.*, 2006). Similarly to eNOS and iNOS, the •NO production rate for nNOS in complex with CaM E84R/E87K was significantly reduced when compared to wild-type CaM, as shown in table 2.3.

Table 2.3 – CaM phosphomimetic/charged and central linker deletion mutant dependent activation of cNOS enzymes [a]

	Neuronal NOS			Endothelial NOS		
CaM protein	NADPH Oxidation %	Cyt *c* Reduction %	•NO Production %	NADPH Oxidation %	Cyt *c* Reduction %	•NO Synthesis %
CaM	100 ± 4	100 ± 3	100 ± 2	100 ± 1	100 ± 4	100 ± 2
CaM (EDTA)	13 ± 4	9 ± 1	NAA[b]	15 ± 3	9 ± 3	NAA
Phosphomimetic /Charge CaMs						
CaM T79D	93 ± 3	105 ± 3	94 ± 3	105 ± 3	86 ± 4	108 ± 3
CaM S81D	89 ± 5	106 ± 5	89 ± 3	107 ± 4	84 ± 5	106 ± 2
CaM T79D/S81D	97 ± 2	111 ± 2	76 ± 3	99 ± 2	80 ± 1	102 ± 3
CaM S101D	80 ± 3	99 ± 3	80 ± 2	100 ± 2	86 ± 4	82 ± 5
CaM E84R/E87K	39 ± 2	31 ± 1	44 ± 3	30 ± 1	18 ± 4	26 ± 3
Central Linker Deletion CaMs						
CaM Δ84	86 ± 3	114 ± 6	101 ± 1	86 ± 5	77 ± 2	80 ± 2
CaM Δ83-84	77 ± 3	118 ± 2	105 ± 3	89 ± 7	92 ± 3	79 ± 1
CaM Δ81-84	82 ± 1	96 ± 2	88 ± 7	58 ± 4	49 ± 4	57 ± 3

[a] The oxyhemoglobin capture assay used to measure the rate of CaM-activated •NO production, the cytochrome *c* assay and the NADPH oxidation assay were performed in the presence of either 3 μM wild-type or mutant CaM protein and either 200 μM $CaCl_2$ or 250 μM EDTA, as indicated. The activities obtained with the respective enzyme bound to wild-type CaM at 25°C in the presence of 200 μM $CaCl_2$ were all set to 100%. The activities for nNOS bound to CaM were 36 min^{-1} (•NO synthesis), 132 min^{-1} (NADPH oxidation) and 1253 min^{-1} (cytochrome *c* reduction). The activities for eNOS bound to CaM were 9 min^{-1} (•NO synthesis), 27 min^{-1} (NADPH oxidation) and 71.1 min^{-1} (cytochrome *c* reduction). The standard deviation was calculated from data obtained in quadruplicates.

[b] NAA – No apparent activity

2.3.3 Effect of CaM central linker deletion mutations on CaM-dependent NOS activation

A 35% decrease in •NO synthesis from iNOS enzyme was detected when in complex with all of the truncated-central linker CaM mutants (Table 2.2). Interestingly, the addition of EDTA to the system resulted in the attenuation of •NO synthesis when iNOS was in complex with each truncated CaM mutant, indicating Ca^{2+}-dependent activation. However, the addition of excess wild-type CaM was able to maintain iNOS enzyme activity.

A decrease in NADPH oxidation or cytochrome c reduction rate was not observed upon removal of residues in the central linker of CaM. These kinetic results indicate that electron

transfer within iNOS is controlled primarily in the FMN domain, transferring electrons to the catalytic heme in the oxygenase domain (Feng *et al.*, 2006).

Unlike the iNOS enzyme, eNOS and nNOS enzymes displayed similar, but not equivalent activation profiles when associated with these three central linker deletion CaM mutants. Shortening the CaM linker region resulted in a slight decrease in eNOS's •NO production by 20-50% (Table 2.3). For nNOS, only CaM Δ81-84 decreased •NO synthesis by 12% when compared to wtCaM. These data are consistent with previous published work, where the activity of various CaM-dependent enzymes were attenuated with the deletion of each residue in the central linker region of CaM (Persechini *et al*., 1989). Likewise, nNOS reductase activities with CaM Δ81-84 followed a similar trend to •NO synthesis (Table 2.3).

2.4 Discussion

Using solved crystal-structures of CaM-eNOS peptide (Aoyagi *et al.*, 2003) and CaM-nNOS peptide (Ng *et al*., PDB 2O60), we were able to provide some proposition for the effects that these CaM mutant proteins have on their association to eNOS and nNOS (Figure 2.4). In terms of eNOS and nNOs, phosphomimetic CaM S101D presented the most significant decrease in catalytic activity; however, this residue does not appear to have any direct interaction with the CaM-binding domain of eNOS and nNOS. It is plausible that this residue maybe be associating with a residue in the flanking region of cNOS. In addition, nNOS also demonstrated a decrease in activation with CaM T79D/S81D. Both of these residue form hydrogen bond with K743 of the rat nNOS CaM-binding domain (position 13, Figure 2.4).

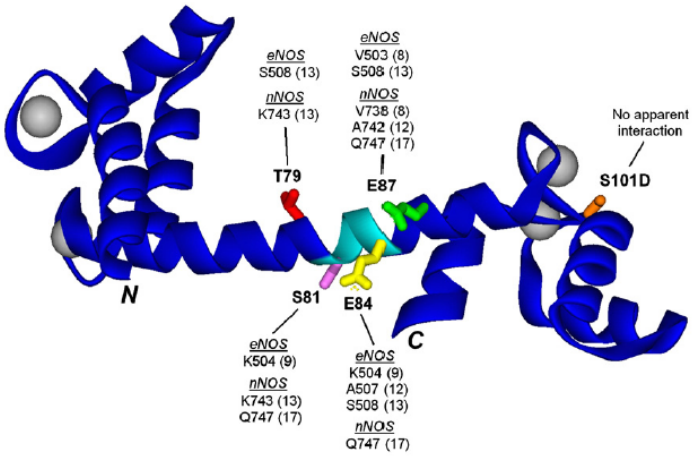

Figure 2.4- Structure of Ca^{2+}-replete wild-type CaM and sequence alignment of the CaM-binding domains of the NOS enzymes. **(A)** The peptide backbone of CaM is shown in blue. The mutation sites in CaM used in this study are highlighted to demonstrate their respective locations in CaM T79 (red), S81 (pink), E84 (cyan), E87 (green) and S101 (yellow). **(B)** Hydrophobic residues found in the NOS CaM-binding motif 1-5-8-14 are highlighted. Acidic and basic residues found in the NOS CaM-binding domains are shown in red and blue, respectively. The model (PDB 1CLL) was generated using ViewerLite 5.0 (Accelrys).

We do not suspect electrostatic interaction between CaM T79D/S81D and nNOS to be the cause of this attenuation. However, we do believe that changes in conformation of CaM's linker region by phosphorylation prohibit optimal association of CaM to the CaM-binding domain of nNOS.

CaM E84R/E87K appears to have the greatest effect on cNOS marked by significant attenuation of the enzyme activity. With respect to eNOS, CaM E84 interacts with K504 of bovine eNOS CaM-binding domain (positions 9) while E87 of CaM interacts with V503 and S508 of eNOS (positions 8 and 13). Consequently, electrostatic repulsion would exist when CaM E84, which interacts with a positive residue K504, is substituted with an arginine residue. In contrast, both E84 and E87 of CaM form hydrogen bonds with Q747 of nNOS (position 17). The only plausible explanation that we can think of that can lead to such attenuation of nNOS activity

by this charged CaM mutant would be the weakening of association between CaM and nNOS by the removal of hydrogen bonds.

Therefore, using both solved crystal structures of CaM bound to eNOS (Aoyagi *et al.*, 2003) and nNOS (PDB 206O) in conjunction with alignment of the NOS CaM-binding domains (Figure 2.4), we have been able to determine the cause of iNOS activity by the current CaM mutants protein. All of the phosphomimetic CaM proteins attenuated iNOS activity; however, based on the alignment of the NOS CaM-binding domain, we suspect that changes in CaM conformation could have destabilized the interaction between NOS and CaM and that electrostatic interaction is disrupted. This can be justified as T79 and S81 of CaM would likely interact predominantly with hydrophobic residues in the human iNOS CaM-binding domain (V522, L523, C526, and M527 as shown in Figure 2.4). Similar to the cNOS enzymes, S101 of CaM would most likely have no direct interaction with the CaM-binding domain of iNOS, but instead with flanking regions in the reductase/oxygenase domain, as previously suggested (Ruan *et al.*, 1996).

The observed NOS Ca^{2+}-dependent activation of cNOS and iNOS by CaM E84R/E87K can be related to a combination of hydrophobic and electrostatic forces. We have mentioned in the result section that E84 and E87 have been shown to interact with Q747 of rat nNOS, using the alignment in Figure 2.4 B. This residue, Q747 of nNOS, correspond to a lysine in the iNOS CaM-binding domain (K531, Figure 2.4 b). Therefore, substitution of a CaM E84 and E87 with positive charge residues will cause a significant electrostatic repulsion between the two proteins. However, this repulsion appears to be hindered by hydrophobic interaction between CaM and NOS in the presence of calcium. Thus, the introduction of EDTA to chelate calcium ions from

CaM weakens the hydrophobic interactions with iNOS that is necessary to overcome the repulsion interaction between K531 (iNOS) and CaM E84R/E87K.

In conclusion, this study has determined that in addition to hydrophobic interactions, electrostatic interaction plays a key role in the Ca^{2+}-independent association of CaM to iNOS. This was accomplished by using a series of CaM mutants where charged residues in the glutamate rich central linker region (residues 82-87) were removed (ex. CaM Δ 81-84), added (CaM S81D) or substituted (CaM E84R/E87K) to measure electron transfer and •NO production in NOS isozymes.

Chapter 3

The effect of Camstatin and Phosphorylated CaM on the activity of Nitric Oxide Synthase

3.1 Introduction

Phosphorylation of CaM results in the activation and modulation of different signal cascades and enzymatic activities within the cell. It has been reported that phosphorylation of S101 of CaM attenuates eNOS activity by 30% (Spratt *et al.*, 2008). On the other hand, CaM phosphorylated (CaM residues T79, S81, S101) by CK-II increases nNOS activity by 300% (Quadroni *et al*., 1998). To date, only 3 (T79, S81, S101) of the 6 amino acid residues within the central linker region and the C-terminal region of CaM that serve as candidates for phosphorylation have been extensively investigated with respect to NOS activity. The present thesis expands on this research by investigating two additional CaM residues that can undergo phosphorylation, Y99 and Y138. These residues are located in the C-terminal domain, in close proximity to the calcium-binding motif. Phosphorylation of Y99 can play an important role in the modulation of cellular process. For example, Y99 undergoes phosphorylation during hypoxia in the cerebral cortex of newborn piglets in response to increased •NO production by nNOS (Mishra *et al.*, 2009a). The authors speculated that the increase in Y99 phosphorylation mediated by •NO serve as a means to up-regulate NOS activity by increasing the affinity of CaM to nNOS.

The project was further expanded by introducing an additional element thought to interact with CaM, Camstatin (Pep-19 peptide, see section 1.2 for details). It has been demonstrated that Camstatin, at high concentrations, attenuates nNOS activity (Slemmon *et al.*, 1996); however, no

current study has evaluated its effect on the eNOS and iNOS isozymes. It is possible that the binding of Camstatin to CaM, in complex with iNOS, may result in the displacement of calcium ions in the CaM C-terminal domain and thereby inhibit iNOS activity. Thus, the phosphorylation of CaM may indirectly serve as a docking element for the binding of Camstatin to CaM in complex with NOS, as shown in Figure 3.1.

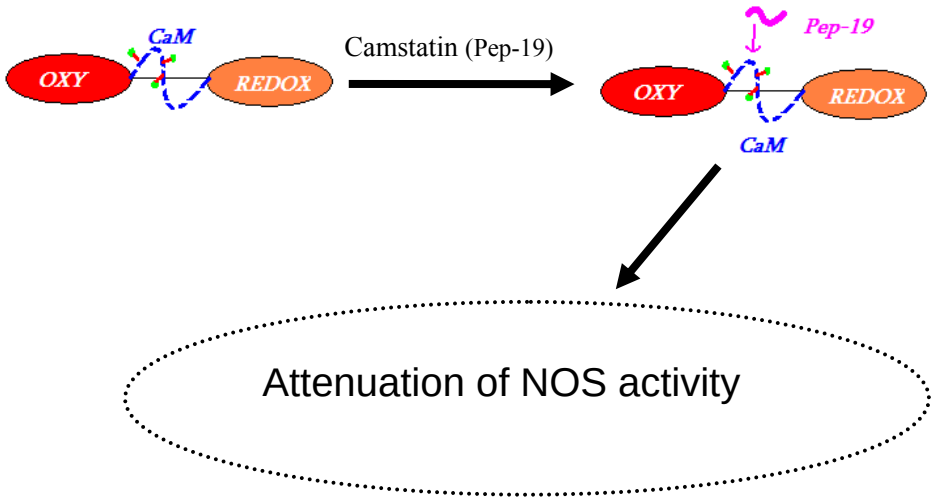

Figure 3.1- Proposed mechanism for NOS inhibition by Camstatin after CaM phosphorylation. Red lines with a green caps that are attached to CaM are a representation of phosphorylated residues. The blue dashed spiral line is a representation of CaM.

The aforementioned hypotheses were examined by generating 6 phosphomimetic CaM proteins: Y99E, Y138E, Y99E/138E, Y99E/138E/S101D, Y99E/S101D, Y138/S101D, and T79D/S81D/S101D. It is important to note that some combinations of these residues are also phosphorylated by the same kinase *in vitro* (see table 1.1). NOS activity was monitored using the oxyhemoglobin capture assay, the cytochrome c reduction assay, and the NADPH oxidation assay (see Figure 2.1). Thereby, the effects of phosphomimetic CaM proteins in conjunction with Camstatin were analyzed based on the activation of NOS.

3.2 Experimental procedures

3.2.1 Mutation of CaM proteins

Vectors (kanamycin resistant pET9d plasmid) coding for phosphomimetic CaM mutant proteins Y99E, Y138E, S101D/Y99E, CaM S101D/Y138E, Y99E/Y138E, Y99E/S101D/Y138E and T79D/S81D/S101D were generated using the QuikChange site-directed mutagenesis procedure (Wang *et al.*, 1999). The primers used in the PCR mutagenesis and cloning reactions for the development of these vectors (CaM mutant Y99E, Y138E, S101D/Y99E, CaM S101D/Y138E, Y99E/Y138E, Y99E/S101D/Y138E and T79D/S81D/S101D) are listed in the Table 3.1.0. Substitution of Tyr, Ser and Thr residues with negatively charged amino acids faithfully mimic the effect of a phosphate ion with respect to charge (Greif *et al.,* 2004).

Table 3.1.0- Primers used for CaM mutagenesis

CaM protein	Primer	DNA Sequence
Mutagenesis		
CaM Y99E	PCaMT99Efr	5' GATAAGGATGGCAATGGCGAGATCAGTGCAGCAGAGCTCCGC
	PCaMT99Erv	5' GCGGAGCTCTGCTGCACTGATCTCGCCATTGCCATCCTTATC
CaM Y138E	PCaMT138Efr	5' GGGGATGGTCAGGTTAACGAGGAAGAGTTTGTA
	PCaMT138Erv	5' TACAAACTCT TCCTCGTTAA CCTGACCATCCCC
CaM Y99E/S101D	PCaMS101D447fr	5' AAGCTCTGCT GCATCGATCT CGCCATTGCC
	PCaMS101D447rv	5' GGCAATGGCG AGATCGATGC AGCAGAGCTT

3.2.2 CaM protein expression and purification

Wild-type CaM and mutant CaM proteins were expressed and purified using affinity chromatography (phenyl sepharose), as previously described (Spratt *et al.*, 2006). The concentration of CaM was determined using protein quantification Lowry Assay. The purity of the proteins was confirmed using ESI-MS and SDS-PAGE.

3.2.3 NOS expression and purification

cNOS enzymes, rat nNOS and bovine eNOS, were expressed as previously described (Roman *et al.*, 1995; Martasek *et al.*, 1996), with the exception that these constructs had an N-terminal polyhistidine tail cloned upstream from their respective start codons. Human iNOS with the deletion of the first 70 amino acids and an N-terminal polyhistidine tail was co-expressed with wild-type CaM or mutant CaM Y99E protein in *E. coli* BL21 (DE3) (Newman *et al.*, 2004). Ammonium sulfate precipitation, metal chelation chromatography, and 2'5'-ADP sepharose chromatography were employed to purify the NOS enzymes as previously described by Dr. Donald E. Spratt (Spratt *et al.*, 2006).

3.2.4 Enzyme kinetics

The assays utilized to measure and monitor the electron transfer rates in NOS included, NADPH oxidation, cytochrome c reduction, and the oxyhemoglobin capture assay, as previously described (Gachhui *et al.*, 1996; Montgomery *et al.*, 2000; Montgomery *et al.*, 2003; Spratt *et al.*, 2007a). Assays were performed in 96-well microtitre plates at 25 °C. Spectral data was recorded using a SpectraMax 384 Plus 96-well UV–visible spectrophotometer and Soft Max Pro software (Molecular Devices, Sunnyvale, CA).

3.2.5 Gel shift mobility assay

Native Gel (15%) mobility shift assays (Sigma Technical Bulletin No. MKR-137, 1986) were performed to study the binding of Camstatin (PEP-19 peptide) with various CaM proteins. Protein interaction between the peptide and CaM is observed as a shift in the mobility of the CaM protein with increasing peptide concentration. In a total volume of 30 μL, wild-type CaM and CaM T79S/S81D (40 μM) were incubated with increasing molar ratios of Camstatin peptide

to CaM protein (0, 1, 4, 8, 15, 29) in binding buffer (100 mM Tris-HCl, pH 7.5, and 0.2 mM $CaCl_2$) at room temperature for 1 hour. Similarly, wild-type CaM and CaM S101D (20 μM) were incubated with increasing molar ratios of Camstatin peptide to CaM protein (0, 0.25, 0.5, 0.75, 1.0, 1.5, 4, 8). At completion of the incubation period, half the volume of each sample was combined with an equal volume of loading buffer, consisting of 50% glycerol and bromophenol blue as a tracer. The sample preparations were then electrophoresed through a 15% non-denaturing polyacrylamide gel containing 0.375 M Tris-HCl, pH 8.8, 4 M urea, and 0.2 mM $CaCl_2$. Gels were run at a constant voltage of 100 V in electrode running buffer consisting of 25 mM Tris-HCl, pH 8.3, 192 mM glycine, 4 M urea, and either 0.2 mM $CaCl_2$. The gels were then stained and visualized using Coomassie Brilliant Blue R-250.

3.3 Results

3.3.1 Protein expression and purification

The final yield of purified phosphomimetic CaM protein was between 10-20 mg/L of medium. Each mutant was found to be about 95% homogeneous based on SDS-PAGE analysis (Figure 3.1.1). Electrospray Ionization-Mass Spectrometry was also conducted to confirm the intactness of the protein as shown in Table 3.1.1.

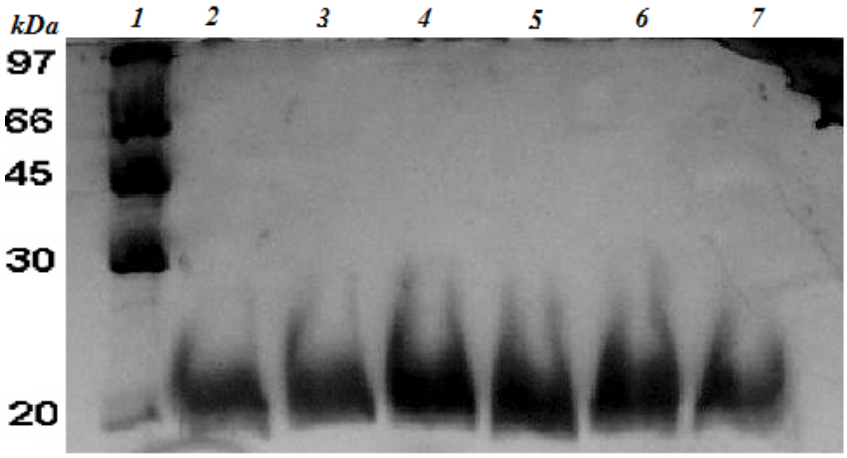

Figure 3.1.1 – 15% SDS-PAGE analysis of purified phosphomimetic CaM proteins.
A 40 µg sample of each purified CaM protein was loaded in a standard SDS-PAGE loading. Lane 1, low molecular mass protein standard(GE Healthcare); Lanes 2 CaM Y99E; Lane 3, CaM Y138E; Lane 4, CaM Y99E/Y138E; Lane 5, CaM Y99E/S101D; Lane 6, CaM Y138E/S101D; Lane 7, CaM Y99E/S101D/Y138E.

Table 3.1.1- Masses of phosphomimetic CaM proteins.

	Mass (Da) [a]	
CaM proteins	Observed	Theoretical [b]
Wild-type CaM	16709	16709
Phosphomimetic CaM		
CaM Y99E	16672	16675
CaM Y138E	16672	16675
CaM Y99E/Y138E	16640	16641
CaM Y99E/S101D	16700	16703
CaM Y138E/S101D	16701	16703
CaM Y99E/S101D/Y138E	16667	16669

[a] Masses of deconvoluted ESI-MS spectra were determined with an accuracy of ± 5 Da.
[b] Calculated masses based upon amino acid sequence.

3.3.2 cNOS activation by phosphomimetic CaM

The oxyhemoglobin capture assay was performed for eNOS and nNOS enzymes to assess the effects that phosphomimetic CaM mutants may have on their activity. The activity of nNOS

associated with each of the phosphomimetic CaM proteins was compared to the relative activity of nNOS in complex with wild-type CaM. Phosphorylation of CaM significantly modified nNOS activity, ranging from 30% to 125%, depending on the specific phosphomimetic CaM protein (Table 3.2). For instance, phosphomimetic CaM Y99E and Y138E resulted in a decrease of nNOS catalytic activity by over 50% when compared to wild-type CaM (Table 3.2). Meanwhile, an increase of nNOS by activity by 25%was observed with phosphomimetic CaM Y99E/S101D and S101D/Y138E. Unlike their effect on nNOS activity, phosphomimetic CaM proteins consisting of a S101D mutation in combination with an Y99E and/or an Y138E mutation caused a decrease in •NO production by eNOS that was two-fold. This result suggests a difference in phosphorylated CaM activation of eNOS and nNOS. Data obtained from the NADPH oxidation and cytochrome c reduction assays reveal that a reduction in the electron transfer rates within the reductase domain does not occur (Table 3.2). This result implies that a decrease in •NO production by cNOS is due to changes in electron transfer to the oxygenase domain from the reductase domain, brought about by specific phosphomimetic CaMs.

Table 3.2- Phosphomimetic CaM mutant dependent activation of cNOS enzymes

	Neuronal NOS			Endothelial NOS		
CaM protein	NADPH Oxidation %	Cyt *c* Reduction %	•NO Production %	NADPH Oxidation %	Cyt *c* Reduction %	•NO Synthesis %
Wt CaM	100 ± 7	100 ± 3	100 ± 2	100 ± 1	100 ± 4	100 ± 1
CaM (EDTA)	15 ± 4	9 ± 1	NAA[b]	15 ± 3	9 ± 3	NAA[b]
Phosphomimetic CaM						
CaM Y99E	106 ± 3	109 ± 2	37 ± 5	93 ± 5	83 ± 2	31 ± 4
CaM Y138E	94 ± 2	103 ± 3	68 ± 4	101 ± 3	75 ± 4	90 ± 1
CaM Y99E/S101D	111 ± 2	96 ± 5	127 ± 3	86 ± 5	98 ± 3	50 ± 3
CaM Y138E/S101D	115 ± 3	102 ± 2	125 ± 5	96 ± 4	98 ± 5	82 ± 1
CaM Y99E/Y138E	99 ± 5	101 ± 4	98 ± 5	92 ± 5	98 ± 3	45 ± 5
CaM Y99E/S101D/Y138E	97 ± 4	94 ± 3	77 ± 3	103 ± 1	98 ± 5	47 ± 2

The standard deviation was calculated from data obtained in quadruplicates.
[b]*NAA- No Apparent Activity*

3.3.3 A gel shift mobility assay of CaM proteins with Camstatin

Gel shift mobility assays were performed to investigate the binding of wild-type CaM and phosphomimetic CaM proteins to Camstatin. A shift in the mobility of wild-type CaM protein with increasing peptide concentration was observed. Weak interactions were detected between Camstatin and wild-type CaM, as well as two of the CaM mutant proteins, T79D/S81D and S101D (Figure 3.2). Future gel shift mobility assays should include Camstatin and other phosphomimetic CaM proteins, such as CaM Y99E and Y138E, to fully assess whether these phosphorylation sites influence CaM-Camstatin interactions.

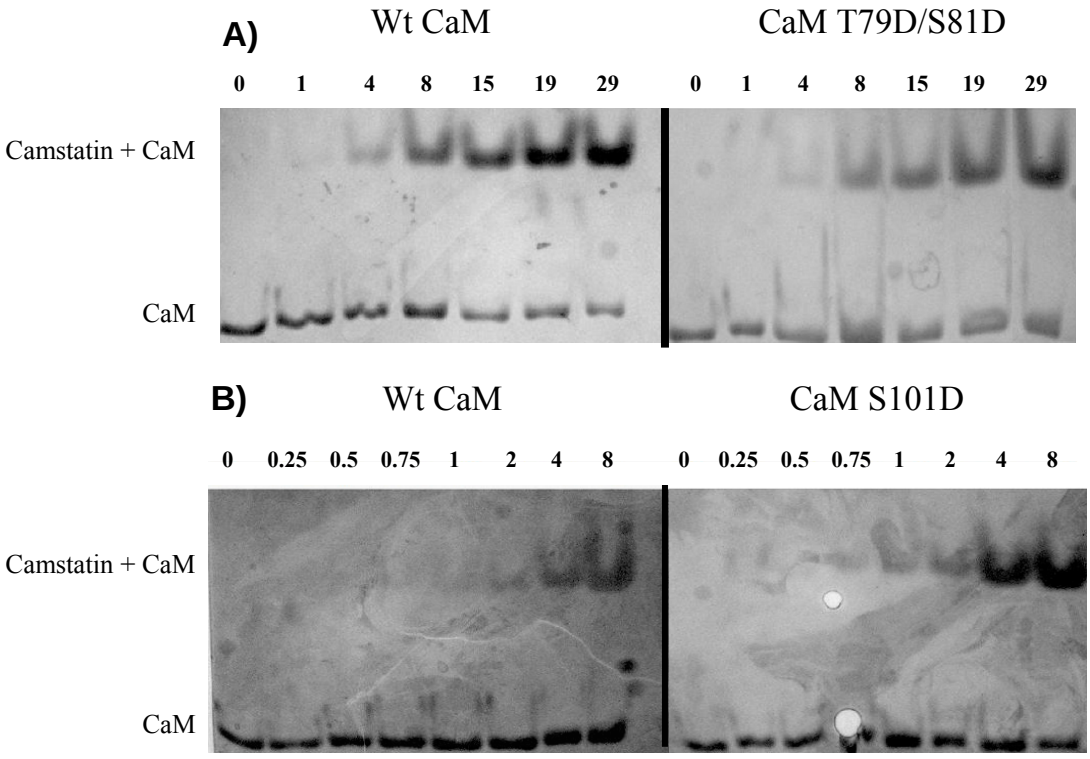

Figure 3.2- Gel shift mobility assay of Camstatin binding to CaM proteins.
A) Wild-type CaM (Wt CaM) (20 μM) and CaM T79D/S81D (20 μM) incubated with increasing molar ratios of Camstatin peptide to CaM (0, 1, 4, 8, 15, 19, and 29) in the presence of 0.2 mM $CaCl_2$. **B)** Wild-type CaM (20 μM) and CaM S101D (40 μM) incubated with increasing molar ratios of Camstatin peptide to CaM (0, 0.25, 0.5, 0.75, 1, 1.5, 4, and 8) in the presence of 0.2 mM $CaCl_2$. Protein separation shown on Native-PAGE (15% acrylamide) containing 0.375 M Tris, pH 8.8, 4 M urea, and 0.2 mM $CaCl_2$, and stained with Coomassie Blue R-250.

3.4 Discussion

The phosphorylation of CaM proteins is an important post-translational modification that has been shown to mediate a number of critical intracellular processes (Spratt *et al*, 2008) Hence, it is of great interest to determine the implications phosphorylated CaM may have on the activation of NOS enzymes. In the present study, data obtained using phosphomimetic CaM proteins indicates that phosphorylation of CaM Y99 residue attenuates nNOS and eNOS activity

by two-fold. Unfortunately, this data is in not in agreement with previous studies by (Corti, *et al.,* 1999). The Corti group did not use phosphomimetic CaM Y99E to assess the activity of nNOS, but instead phosphorylated CaM using PTK-III kinase *in vitro* (see at table 1.1). Although PTK-III targets CaM Tyr 99 for phosphorylation, a small fraction (~15%) of CaM Tyr 138 was also phosphorylated in their study. This was determined using ESI-Mass spectroscopy. Nevertheless, the author observed a 3 fold increase in nNOS activity by CaM phosphorylated at Tyr 99 and/or Y99/Y138. It is very plausible that phosphomimetic residues, employed in this thesis, Y99E and Y99E/Y138E of CaM are not mimicking the effects of an actual phosphorylated tyrosine residue of CaM. To determine whether the reduction in NOS activity is due to electrostatic interaction resulting from the Glu side chain, or changes in the conformation of CaM arising from the CaM mutation, future experiments must be performed with CaM mutants containing a substitution of Tyr 99 with Gln instead of Glu. Therefore, if a reduction in the nNOS activity by CaM with a Gln 99 substitution is equivalent to the one by CaM Glu 99, it can be concluded that the phosphomimetic CaM-Y99E does not mimic CaM with phosphorylation at Y99. It is possible that the Corti group may have made a mistake in their analysis. This can be justified by examining the crystal structure of Holo-CaM. The phenol group of CaM Y99 is located about 5 Å away from Asp 131, Asp 133 and Asp 137.

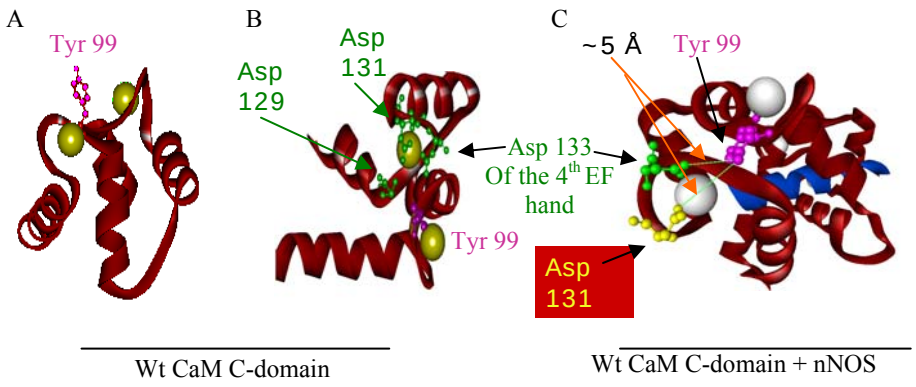

Figure 3.3- Structural comparison of the C-terminal domain of Ca^{2+}-CaM. Structures **A)** and **B)** represent the C-terminal domain of CaM with Tyr 99 colored in purple with Asp 131, 133, and 137 colored in green. **C)** C-terminal domain of wild-type CaM with nNOS peptide (colored in blue). Asp 133 is colored in green with Tyr 99 colored in purple and Asp 131 colored in yellow. The distance between Asp 133 and Tyr 99 of CaM is 5Å away. The yellow/white spheres represent calcium ions. The model was created using coordinates for Holo-CaM (Chattopadhyaya *et al.*, 1992) PDB 1CLL and PDB NO60 for CaM with NOS peptide. Models were generated using ViewerLite 5.0 (Accelrys).

Therefore, the addition of a negatively charged phosphate ion in the vicinity of a negatively charged aspartic acid cluster may result in an electrostatic repulsion that disrupts the required binding of calcium ion to the 4th EF-hand motif of CaM, thus modifying its entire conformation. One way of preventing the 4th EF-hand motif of CaM from binding to calcium ions is by substituting the aspartic acid 131 with alanine residue to disrupt the biding of 4th EF-hand motif to calcium ions (Spratt *et al,* 2007 b). As a result, CaM that can not bind to calcium ion on the 4th EF-hand motif will not be able to fully activate nNOS. This is based on studies by Spratt *et al,(2007b).* Unfortunately, direct interactions between CaM Y99 and residues of the cNOS CaM-binding domain are unknown based on crystal structure of CaM bound to NOS CaM-binding domain. It is plausible that Y99 associates with NOS residues outside of the CaM-binding domain, such as the oxygenase domain. Neither the NADPH nor the cytochrome c assay, which monitor electron flow in the reductase domain of NOS, displayed significant changes with

any of the phosphomimetic CaM proteins when compared to wild-type CaM (Table 3.2). However, unlike the eNOS enzyme, where CaM Y99E variants attenuated the enzyme activity by two-fold, nNOS was not affected to a significant degree by this phosphomimetic residue when in coexistence with other phosphomimetic residues, such as S101D or Y138E.

Disrupting the native conformation of CaM by phosphorylation to modulate the activity of target enzymes could serve many functional purposes in the cell. For example, Tyr 99 phosphorylation in the cerebral cortex of newborn piglets during hypoxia could serve as a defensive mechanism by neurons in response to increased •NO production by nNOS (Mishra *et al.*, 2009b).

On the other hand, CaM Tyr 138 is located 2 Å away from CaM Glu 82 when CaM is bound to Ca^{2+}. However, this distance is extended to ~6 Å when CaM is bound to either the nNOS or eNOS CaM-binding domain peptide. Therefore, phosphorylation of CaM Y138 should not result in a significant change in cNOS activity, although a 30% reduction in •NO synthesis by nNOS is observed.

Binding and structural disturbances between CaM and its target protein upon Camstatin binding have already been demonstrated. Camstatin, at 40-fold excess to CaM, can compete with NOS for the binding of CaM, even though the binding affinity of CaM to NOS is 40-fold higher than it is to Camstatin. Therefore, phosphorylation of CaM may increase the binding affinity of CaM to Camstatin or reduce CaM's affinity for NOS. With this in mind, we performed several Gel Shift Mobility Assays to analyze the binding stoichiometry of Camstatin to some of the previously studied phosphomimetic CaM proteins (S101D and T79D/S101D). Originally we attempted to saturate CaM with 8-fold excess Camstatin; however, this was not the case. The low binding affinity of Camstatin to wild-type CaM is observed when CaM could not be saturated by

40-fold excess Camstatin (Figure 3.2). This supports the previous notion made earlier that the binding affinity of Camstatin to CaM is very weak and that phosphorylation of CaM in the C-terminal domain may increase the binding affinity.

The next approach is to investigate the effect phosphomimetic CaM variants with Camstatin in the activation iNOS.

Chapter 4

Protein trafficking of Apo-CaM in live mammalian cells

4.1 Introduction

Calmodulin (CaM) is one of the most abundant proteins in the eukaryotic cell, constituting up to 1.0% of the total eukaryotic cell proteins (Means *et al*, 1982). Depending on the cell cycle and the cell type, CaM is observed to localize in both the cytoplasm and the nucleus of eukaryotic cells. For instance, it has been determined that CaM proteins, in smooth muscle cells, are localized in the cytoplasm during cell resting state (Thorogate *et al*, 2004) Changes in the localization of CaM are caused by spikes of intracellular calcium concentrations in response to a stimulus (Zavortink *et al.*, 1983; Teruel *et al.*, 1999). Stimulation of the cell followed by an influx of the calcium ions results in the translocation of CaM into the nucleus by an unknown shuttle protein (Thorogate *et al*., 2007).

Little is know about the spatial distribution of CaM within the cell. Nonetheless, Torok's group was able to illustrate the spatial distribution of CaM in sea urich zygote before and after fertilization (Torok *et al.*, 2002). In their study, CaM was observed to localize in the nucleus of the zygote prior fertilization, and on the chromosomes during the fertilization process (Torok *et al.*, 2002).

Persechini and collaborators revealed that CaM was limiting in the cell with an estimated concentration 20 μM (Persechini *et al,* 2002). Changes in concentration and spatial distribution of CaM inside the cell can play a vital role in modulating cellular processes. For example, a decrease in CaM concentration in the cell can arrest the cell cycle at the G_1 phase (Persechini *et*

al., 2002). Furthermore, the limited amount of CaM in the cell causes competition between target-proteins and permits selective activation of cellular processes. Post-translational modification of either target-proteins or CaM itself can have a great impact on CaM dependent signaling pathways. For instance, phosphorylation of CaM can change its binding affinity for certain target-proteins, thus allowing it to selectively activate various enzymes or cellular processes (Persechini *et al*, 2002).

4.1.1 Apo-CaM in mammalian cells

For decades, it was believed that CaM can only bind to its target protein in a calcium replete-form. However, current research has emphasized the functionally important role of Apo-CaM. In addition to the 8 known cytoplasmic Apo-CaM target proteins, Apo-CaM can also associate with the cell membrane and other cellular compartments, such as the nucleus, mitochondria and sarcoplasmic reticulum (Figure 4.1) (Thorogate *et al*, 2004; Maier *et al.*, 2006).

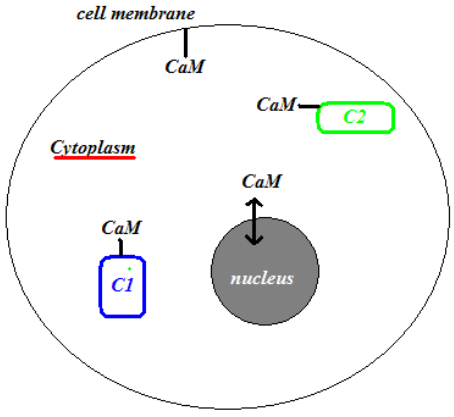

Figure 4.1- Schematic representation of the compartmental association of Apo-CaM within a cell. C1 refers to the sarcoplasmic reticulum; C2 refers to the mitochondria.

It is reported that 99% of CaM in the adult cardiac myocyte is bound to target proteins, either in its Apo-form or with some calcium bound to it (Maier *et al.*, 2006). Upon calcium induction, Apo-CaM favors the binding and activation of localized cytoplasmic or membrane target proteins in its vicinity (Maier *et al.*, 2006). Intrigued by these observations, we decided to investigate the uptake and distribution of Apo-CaM in various mammalian cell lines. This work was to be accomplished by labeling the Apo-CaM protein with a fluorescent marker and coupling it to cell-membrane translocation vector.

As a result, Apo-CaMs were generated by substituting an aspartic acid in the EF-hand motif with an alanine to prevent the binding of calcium ions (Figure 4.2) (Table 4.1).

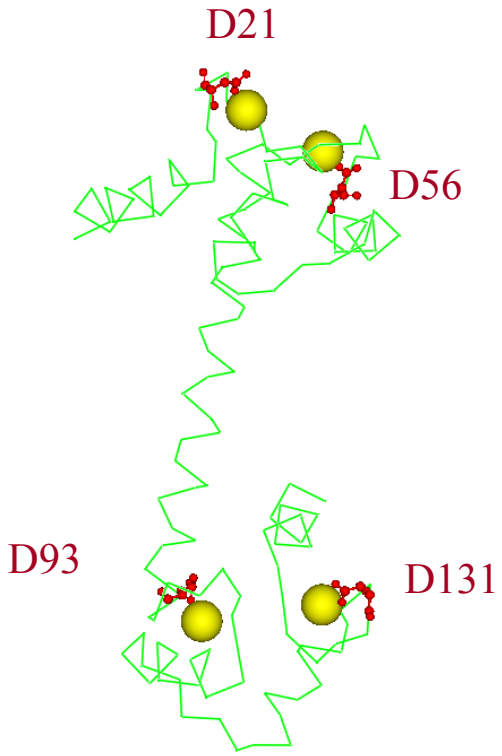

Figure 4.2- Schematic diagram of CaM protein. Key calcium binding residues in each EF-hand motif is colored in red. Modification of each aspartic residue to alanine prevents the binding of calcium to the EF-hand motif.

Table 4.1- A list of Apo-CaM mutants.

CaM mutant [α]	Category	Type of Modification
CaM_{12}	Partial Calcium-deficient	D21A, D56A
CaM_{34}	Partial Calcium-deficient	D93A, D131A
CaM_{1234}	Apo-CaM	D21A, D56A D93A, D131A

[α] These proteins have also been modified to contain two Cysteine (Cys 34 and Cys 110) residues for fluorescence labeling and TAT coupling. The numerical values preceding "CaM" correspond to the EF-hand motifs that are not capable of binding to calcium ions. For example, CaM_{12} can only bind to calcium ions in the 3rd and 4th EF-hand of the CaM protein.

Furthermore, to monitor protein trafficking of Apo-CaMs in the cell, a cysteine residue was incorporated (T34C) for labeling purposes. In this case, Apo-CaM proteins were labeled with a thiol reactive probe, such as Texas Red (Figure 4.2.1).

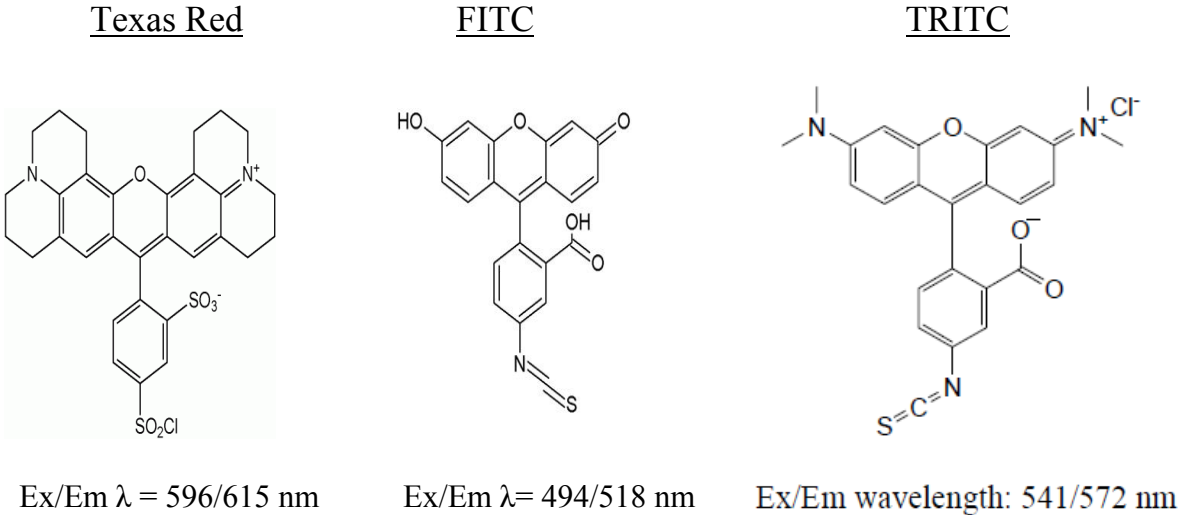

Figure 4.2.1- Fluorescent probes. These probes were used in the labeling of CaM proteins (Texas Red and TRITC) and TAT peptide (FITC)

In addition, a second cysteine residue (C110) was also incorporated in CaM proteins to serve as a reactive site for TAT coupling. TAT peptides will serve as a delivery system to introduce Apo-CaMs into the cytoplasm of mammalian cells with great efficiency and low

cellular toxicity (see Table 1.2 for TAT peptide sequence). However, since TAT peptides contain a nuclear localization sequence (NLS) that shuttles attached cargo molecules to the nucleus, it was necessary to couple peptide Apo-CaMs to TAT peptide by a disulfide bridge. The internalization of the Apo-CaM-TAT fusion protein in the cytoplasm will result in the reduction of the disulfide bridge by intercellular glutathione, thus liberating CaM from the TAT peptide (Fischer *et al.*, 2005). This modification should allow Apo-CaM to freely interact with other cellular compartments and proteins upon cellular internalization, while permitting TAT peptide to continue on its course to the nucleus.

The TAT peptides used in this study were also labeled with a fluorescein isothiocyanate (FITC) fluorophore (Figure 4.2.1), for tracking purposes (Figure 4.3).

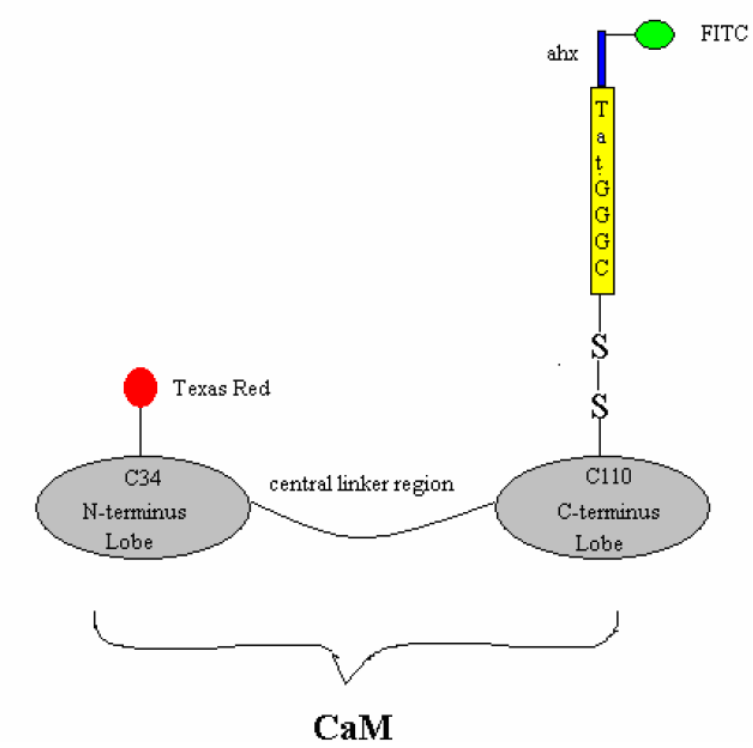

Figure 4.3- Illustration of labeled TAT peptide-CaM fusion protein. The color of each component appears in parenthesis after its identification: aminohexanoyl linker, represented as ahx (blue), FITC probe (green), TAT peptide (yellow), CaM (grey) and Texas Red probe (red).

Three different cell lines were employed in this investigation to monitor fluorescently active CaM proteins intracellularly. These cell lines included mouse Embryonic Stem Cells (mESCs), Human Neuronal Glioma Cells (HNGCs), and Human Umbilical Vein Endothelial Cells (HUVECs). These cell lines were chosen because they differ in their functional specialization and they were made readily available to us by our collaborator, Dr. E. Jervis (Chemical Engineer, University of Waterloo). In addition, using functionally different cells would allow us to compare and contrast protein trafficking of Apo-CaM in cells with different cell cycles and metabolic properties.

To maximize the product yield of the CaM-TAT fusion construct, an amine reactive Tetramethyl Rhodamine Iso-Thiocyanate (TRITC) fluorophore was substituted for the Texas Red dye (Figure 4.2.1). This substitution liberated a second cysteine residue in CaM that was used to increase TAT-CaM coupling efficiency by reducing the number of purification steps.

4.2 Experimental procedures

4.2.1 Protein expression and purification of CaM

Apo-CaM proteins (CaM_{1234}, CaM_{12} and CaM_{34}), a generous gift from Dr. J. Adelman, were modified to contain two thiol groups by substituting T34 and T110 with cysteine residue for Texas Red labeling and TAT-FITC coupling. The protein expression and purification procedure for Apo-CaM is summarized in section 2.2.2. ESI-MS and SDS-PAGE analysis was used to evaluate the purity of the proteins.

4.2.2 Rhodamine labeling of CaM

CaM proteins and rhodamine dyes (Texas Red or TRITC) were transferred into labeling buffer (0.1 M sodium bicarbonate, pH 9.0) via gel filtration using a Sephadex G-25 PD-10 column (Amersham Biosciences), as previously described by Lang *et al.* (2005), to remove traces of Tris-buffer and DTT. The concentrations of the CaM proteins were estimated to be about 8 mg/mL based on UV spectroscopy analysis. The labeling process was performed as described by the manufacturer (Molecular Probes, Eugene, OR, USA) with the exception that for every mole of CaM present in the reaction, 2-3 moles of TRITC was added. Excess TRITC was removed via gel filtration using a Sephadex G-25 PD-10 column (Amersham Biosciences), equilibrated with 100 mM phosphate buffer, pH 7.4, to ensure that all non-covalently linked dye was removed from the labeled CaM proteins. The flow-through was collected in 500 µL fractions. Fractions that contained CaM were pooled and analyzed by ESI-MS to confirm successful TRITC or Texas Red labeling of each CaM protein. The thioethers in CaM do not react with amine reactive TRITC or Texas Red molecules. The remainder of the pooled fraction was stored at -80ºC for subsequent experiments.

4.2.3 CaM-TAT coupling

The TAT-FITC peptide (FITC-AHX-YGRKKRRQRRRGGGC[NPYS]-NH_2; MW 2490 Da) was purchased from ANASPEC (Fremont, California, USA). A coupling efficiency of 100% for TAT-FITC and free thiol groups of CaM requires that the CaM protein samples be completely devoid of Dithiothriotol (DTT) and Tris buffer. This was achieved by transferring CaM proteins into a coupling buffer (100 mM Phosphate buffer, pH 6.3) by gel filtration using a Sephadex G-25 PD-10 column (Amersham Biosciences). CaM is then reacted with 4 fold excess

TAT-FITC to CaM protein to ensure maximum coupling efficiency. The reaction was carried out at room temperature for 12 hours on a shaker. The sample was then washed three times with deionized water using a 10 kDa cut-off spin column (Pall Scientific) to remove excess unbound FITC-TAT. ESI-MS was used to confirm FITC-TAT labeling of each CaM protein.

4.2.4 Fluorescence imaging of live cells

mESCs, HUVEC, and HNGCs were adhered to the surface of gap chambers in 500 μL medium (DMEM/F12). Added to each separate chamber was incubated with one of the following samples: CaM-TRITC, TAT-FITC, TRITC-Lysine, and FITC-TAT-CaM-TRITC with a total concentration of 20 μM. The chambers were incubated for 2 hours at 37˚C. Following incubation, the cells were washed twice with 500 μL of growth media (Neurobasal Expansion 21103 or DMEM) and imaged at 400X magnification using a fluorescence microscope (Zeiss Axiovert 200M) to detect FITC and TRITC fluorescence. The FITC fluorophore was excited at 485 ± 20 nm and detected with a 515-565 nm bandpass filter. The TRITC or Texas Red fluorophore was excited at 560 ± 50 nm and detected with a 645 ± 75 nm bandpass filter.

4.2.5 PREP-4 purification procedure

Unfortunately, it was discovered that the acquired images of all three cells (mESC, HUVEC, HNGC) incubated with rhodamine labeled CaM were contaminated with non-specific TRITC/Texas Red emission from within the cells. From previous experiments, involving fluorescent imaging of cells incubated with FITC-labeled CaM, we know that CaM does not enter the cell without a translocation vector (Figure 4.4). Hence, cells incubated with CaM-Texas Red (a rhodamine dye) or TRITC dye were not expected to fluoresce, nevertheless, they

did (Figure 4.3.1). A possible explanation for this may be that a significant amount of TRITC and Texas Red molecules broke free from the CaM proteins and became internalized by the cell (Rashid and Horobin, 1990).

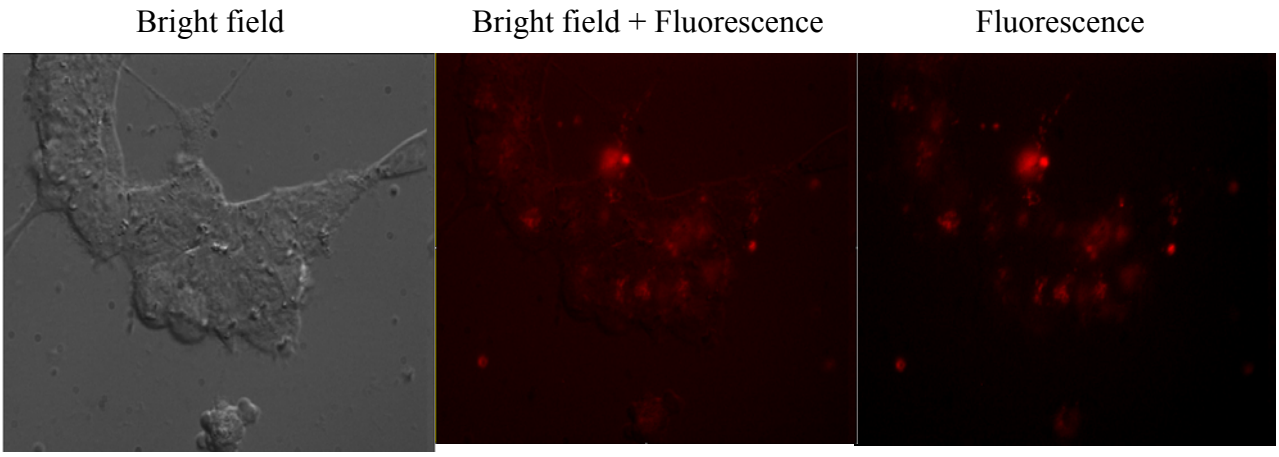

Figure 4.3.1- Cell imaging of HUVECs-2. HUVECs imaged at 400X magnification 2 hours after CaM-Texas Red incubation (20 µM) at 37ºC**.** The cells were washed twice with 500 µL of medium to remove CaM-Texas Red proteins and then re-suspended with 500 µL of fresh medium (DMEM by Invitrogen). Fluorescence emission of Texas Red is observed within the cell.

Alternatively, the rhodamine dyes may have promoted the shuttling of CaM across the cell membrane. This can be tested by labeling CaM with both FITC and Rhodamine probe. Therefore, if a co-localized of FITC and rhodamine fluorescence emission is observed, we can make a conclusion that the rhodamine dye is acting as shuttle vector since we know that free FITC probe can permeate the cell membrane and that the observed FITC emission from the cell has to be due to the internalization of CaM by rhodamine probes.

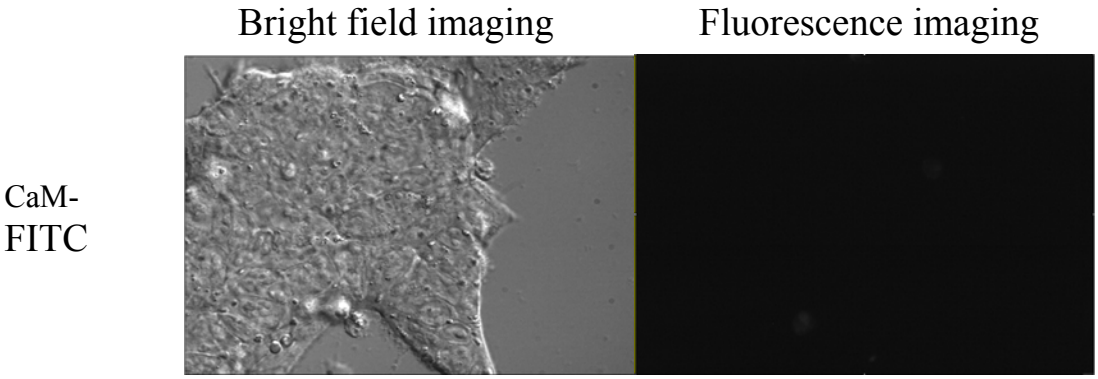

Figure 4.4- Cell imaging of HUVECs. HUVECS were imaged at 400X magnification, two hours after FITC-CaM (40 uM) incubation**.** The cells were washed twice with 500 µl of DMEM medium to remove unbound CaM-FITC residues and then overlaid with 500 µl of fresh DMEM media (Invitrogen), The fluorescence FITC emission is observed form the chambers indicating that the cells did not uptake CaM-FITC protein.

In an attempt to eliminate the non-specific fluorescence of TRITC, a protocol was devised to remove free residual rhodamine molecules from the CaM-TRITC samples. The procedure consisted of a 4-step purification process, referred to as PREP-4 in this thesis. Step one employed size exclusion chromatography in a Sephadex G-25 PD-10 column (Amersham Biosciences) with a 10 kDa molecular weight cut-off to separate TRITC-CaM (Mw ~18000 g/mol) from free TRITC molecules (Mw ~ 500 g/mol). In this stage excess TRITC dye is localized at the top of the column (Figure 4.5 A) The collected eluate was then mixed with a hydrophobic adsorbent mesh (non-polar polystyrene Biobeads SM-2; Biorad) for 30 minutes in 10 mM EDTA. EDTA serves to chelate calcium from CaM to prevent non-specific binding of TRITC probe to the hydrophobic pockets of CaM. Meanwhile, the beads capture free TRITC from the sample by hydrophobic interactions. The supernatant was collected from the hydrophobic adsorbent mesh, which turned pink, indicating that the dye had bound to it (Figure 4.5 B). In the third step, the collected supernatant was transferred onto a phenyl sepharose resin column, equilibrated with buffer C (10mM Tris-HCl, 10 mM EDTA, pH 7.5 @ 4^{o}C). Phenyl

sepharose resin can only bind to free TRITC probes in the presence of EDTA by preventing the exposure of CaM's hydrophobic pockets that is required for the binding of CaM to the resin (Figure 4.5 C). A 10 ml fraction was collected from the column and loaded onto a 15 mL Viva Spin column with a 10 kDa molecular weight cut-off and concentrated to a final volume of 1 mL. The color pink was not observed in the effluent at this stage, indicating that the sample was free of unbound dye (Figure 4.5). The purified sample was then loaded into a gap chamber, containing 10^6 HNGCs, at a final concentration of 20 μM TRITC-CaM, and incubated for 1 hour at 37 ºC. The cells were then washed twice with 500 μL of neuronal basal media and imaged with a fluorescent microscope (Zeiss Axiovert 200M) at 400X magnification.

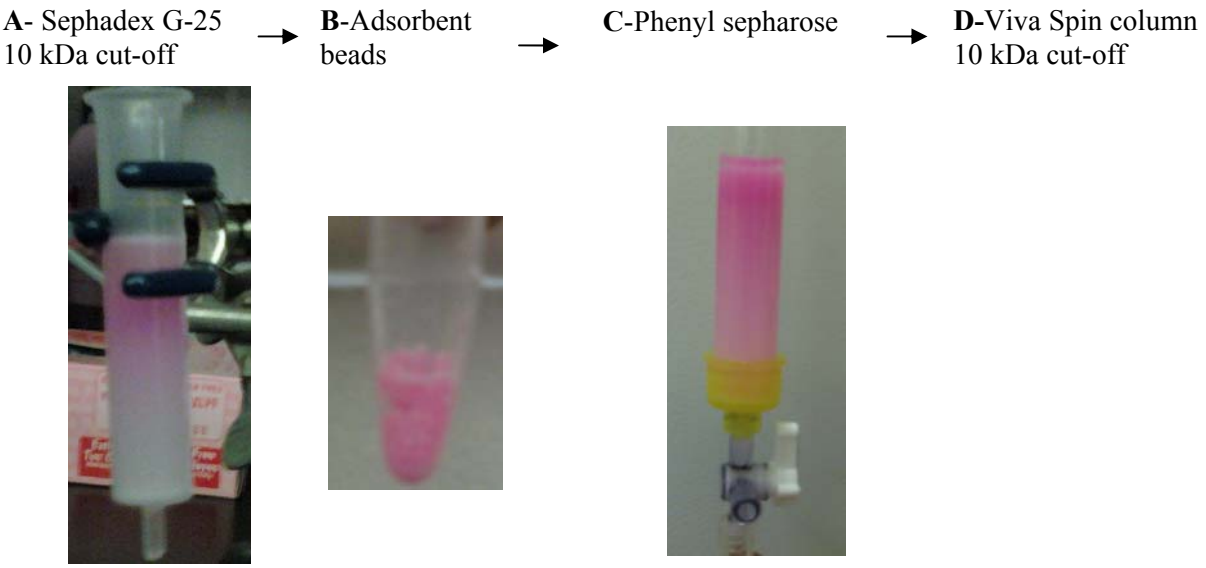

Figure 4.5 - Prep-4 purification of CaM-TRITC. A-B denotes the four steps performed to eliminate unbound TRITC molecules from CaM-TRITC sample. **A**) Employs the use of a gel filtration gravity column; **B)** utilization of hydrophobic binding beads; **C**) hydrophobic binding resin is used to remove free TRITC; **D**) gel filtration spin column is used to further purify the protein from free TRITC. Pink coloration in the purification apparatus is the TRITC probe.

4.3 Results

4.3.1 Characterization of mutant CaM proteins

The purity of CaM was determined to be over 95% homogeneous by SDS-PAGE analysis (Figure 4.6). The actual molecular weight of Apo-CaM protein was confirmed to be the same as the predicted theoretical weight by ESI-MS (Table 4.2). The labeling efficiency of CaM T110C with TRITC fluorophore was greater than 100%, as assessed by ESI-MS (Figure 4.7A). A fraction of CaM T110C had two to three TRITC fluorophores attached to it. Coupling efficiency of TRITC-CaM T110C with TAT-FITC was determined to be 100% by ESI-MS analysis, as shown in Figure 4.7 B and Table 4.2.

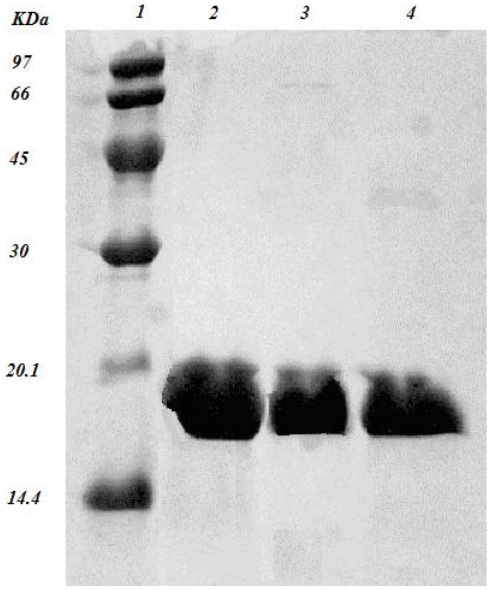

Figure 4.6- 15% SDS-PAGE analysis of purified Apo-CaM proteins.
A 50 µg sample of each purified CaM protein was loaded with standard SDS-PAGE loading buffer containing 1 mM EDTA. *Lane 1*, low molecular mass protein standard (GE Healthcare); *Lane 2*, CaM_{1234} T34C/T110C; *Lane 3*, CaM_{12} T34C/T110C; and *Lane 4*, CaM_{34} T34C/T110C.

Table 4.2 Masses of un-labeled and labeled Apo-CaM proteins

	Mass (Da)	
CaM proteins	Observed	Theoretical
CaM T110C	16711	16712
Calcium Deficient CaMs		
CaM 12-T34C/T110C	16618	16620
CaM 34-T34C/T110C	16618	16620
CaM 1234-T34C/T110C	16533	16534
Labeled CaM		
TRITC-CaM T110C	17151	17153
TRITC-CaM T110C-TAT-FITC	19928.5	19930

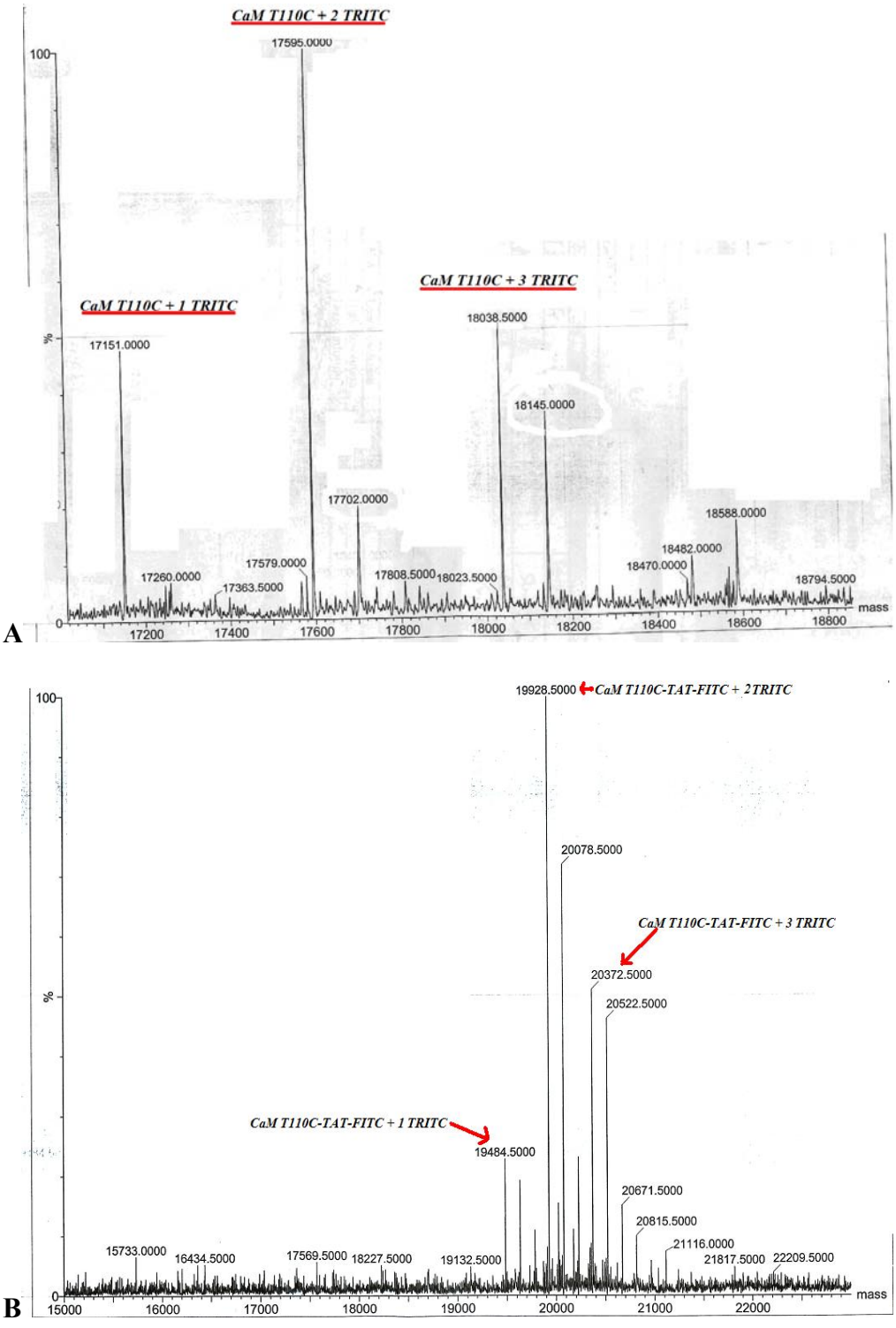

Figure 4.7- ESI-Mass spectroscopy of CaM. Mass spectral data for **A)** CaM T110C-TRITC**,** showing 1, 2 and 3 TRITC fluorophores coupled to it, and **B)** CaM T110C-TRITC**-**TAT-FITC protein variants coupled with a single TAT-FITC peptide.

4.3.2 Fluorescence imaging of live cells

mESCs, HUVECs and HNGC were imaged using a fluorescence microscope at 400X magnification after FITC-TAT peptide addition (Figure 4.8). Based on the acquired FITC fluorescence data, HNGC was the only cell line that showed significant association with TAT peptides. The mESCs and HUVECs only displayed FITC fluorescence in dead or dying cells. However, it was too difficult to distinguish between internalized FITC-TAT peptide and membrane associated FITC-TAT peptide using this technique. In future experiments, it would be of value to perform a mild trypsin (1mg/mL) treatment on the cells to remove non-specific binding of TAT peptide to cell membrane constituents, prior to imaging (Richard *et al.*, 2003). Also, confocal microscopy can aid in confirming the localization of TAT peptide, relative to the cell in 3D.

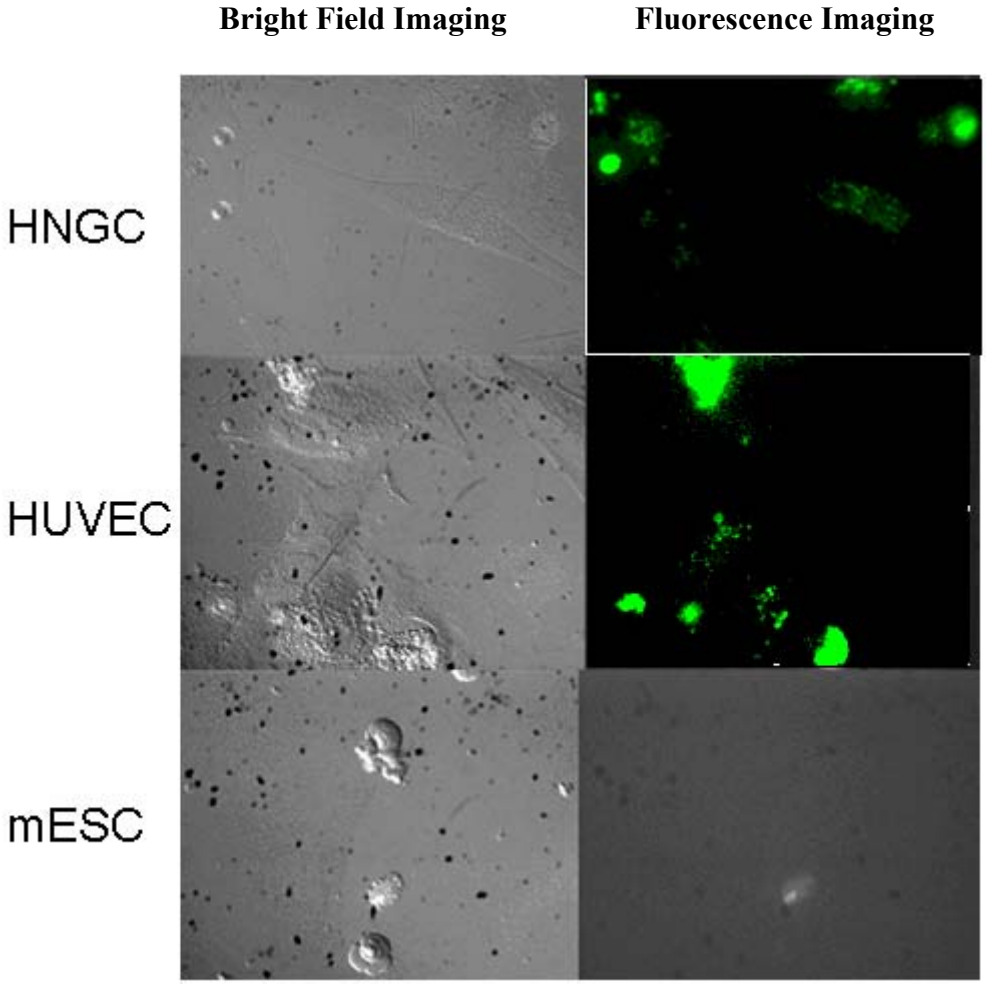

Figure 4.8- Cell imaging of mammalian cells. Images at 400X magnification of HNGCs, HUVECs, and mESCs two hours after FITC-TAT incubation (20 µM)**.** The cells were washed twice with 500 µL of DMEM medium to remove unbound TAT-FITC residues and then overlaid with 500 µL of fresh DMEM medium (Invitrogen, Carlsbad, California).

4.3.3 Fluorescence imaging of live cells with PREP-4 purification process

HNGCs incubated with 20 µM TRITC-CaM after carrying out the PREP-4 purification is still contaminated with free rhodamine, as TRITC emission was detected with the fluorescence microscope (Figure 4.9). It is still unclear as to whether the observed fluorescence in the acquired images is derived from unbound TRITC probe or from CaM-TRITC in the cell. In

future experiments, solving this conundrum entail labeling CaM with both TRITC and FITC probes, and identifying their localization with respect to the HNGCs. Since previous experiments have shown that the FITC probe can not be internalized by the cells, co-localization of both fluorescence emissions will be an indication that the TRITC probe is acting as a shuttle, delivering CaM into the cell.

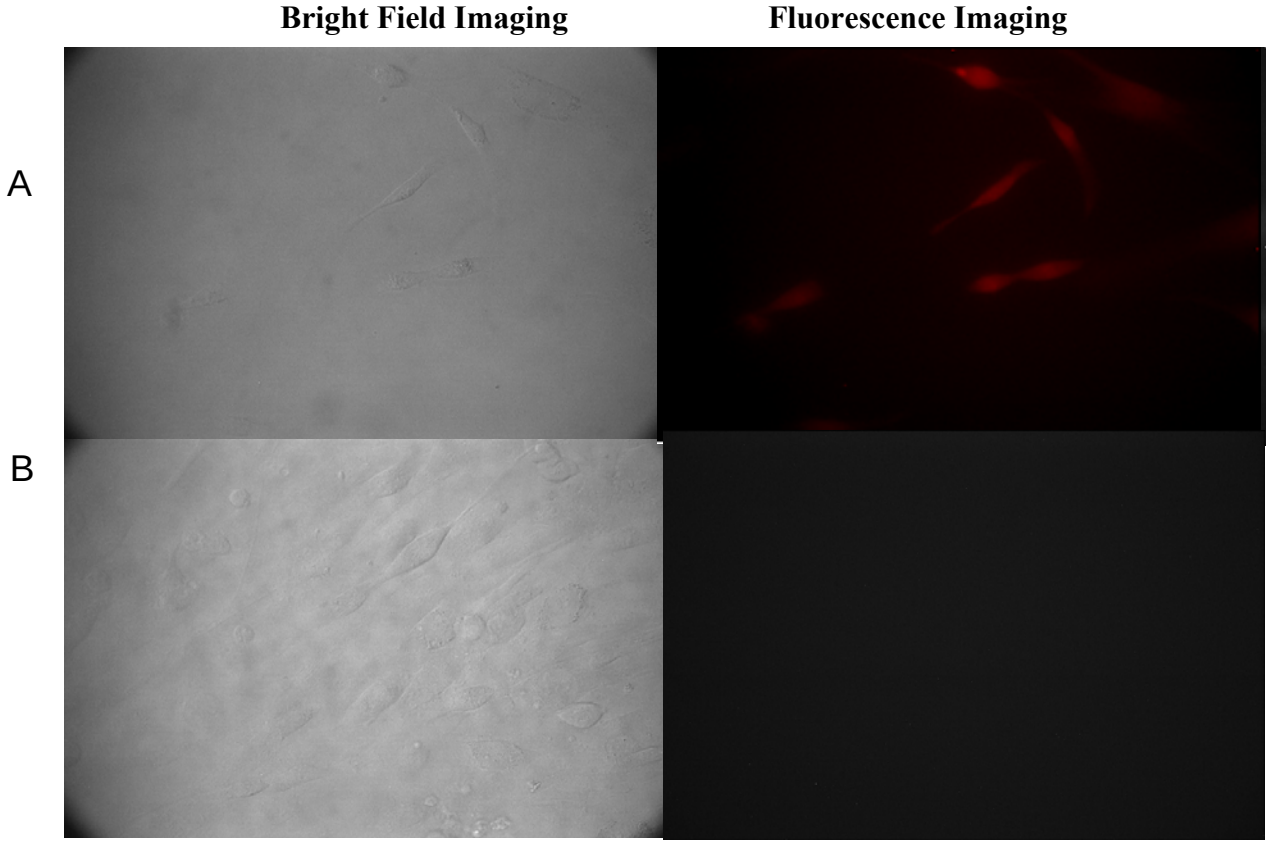

Figure 4.9- Cell imaging of HNGCs with Prep-4 CaM-TRITC. Images at 400X magnification of HNGCs, two hours after CaM-TRITC incubation (40 μM)**.** A) TRITC-CaM purified by the PREP-4 method, and B) control cell sample (without TRITC-CaM). The cells were washed twice with 500 μL of basal medium to remove unbound TRITC-CAM residues and then overlaid with 500 μL of fresh medium.

4.4 Discussion

Of the four cell lines tested for TAT-FITC peptide internalization, only the HNGCs exhibited FITC emission (Figure 4.8). However, it was never confirmed as to whether the observed FITC emission within the cells resulted from TAT internalization or an artifact of non-specific interactions between TAT and cell membrane constituents. Nonetheless, HUVECs and mESCs were not capable of up-taking FITC-TAT peptide into the cell. Although TAT peptide has been previously established as a CPP capable of penetrating all cell types, recent studies have emerged with contradicting evidence and propose that different cell types, differing in their membrane composition, also differ in the degree of interaction with TAT (Fonseca *et al.*, 2009). Further complicating things, many reported results contain artifacts arising from cell fixation procedures that result in the permeabilization of the cell membrane and passive entry of TAT into the cell (Fischer *et al.*, 2005). It has been reported that thiol/disulfide exchange reactions can occur between CPP residues and thiols on the cell-surface, promoting CPP internalization (Aubry *et al.*, 2009). It is possible that the TAT-FITC peptide used in this study may be interacting with cell membrane thiol groups via a cysteine residue, leading to its entry into the cell.

Another source of contamination, hindering this study, was caused by the rhodamine fluorophore. Despite the notion that TRITC- and Texas Red-labeled CaM is impermeable to the cell membrane, non-specific rhodamine emission was detected within the cell, even after several wash steps (Figure 4.9). Additional purification steps are required to avoid this contamination; otherwise, it may be necessary to resort to the use of a different fluorophore label that does not freely cross or interact non-specifically with the cell membrane.

References

Alderton, W.K., Cooper, C.E., and Knowles, R.G. (2001). Nitric oxide synthases: structure, function and inhibition. Biochem J *357*, 593-615.

Aoyagi, M., Arvai, A.S., Tainer, J.A., and Getzoff, E.D. (2003). Structural basis for endothelial nitric oxide synthase binding to calmodulin. EMBO J *22*, 766-775.

Aubry, S., Burlina, F., Dupont, E., Delaroche, D., Joliot, A., Lavielle, S., Chassaing, G., and Sagan, S. (2009). Cell-surface thiols affect cell entry of disulfide-conjugated peptides. FASEB J *23*, 2956-2967.

Benaim, G., and Villalobo, A. (2002). Phosphorylation of calmodulin. Functional implications. Eur J Biochem *269*, 3619-3631.

Dickerson, J.B., Morgan, M.A., Mishra, A., Slaughter, C.A., Morgan, J.I., and Zheng, J. (2006). The influence of phosphorylation on the activity and structure of the neuronal IQ motif protein, PEP-19. Brain Res *1092*, 16-27.

Drum, C.L., Yan, S.Z., Bard, J., Shen, Y.Q., Lu, D., Soelaiman, S., Grabarek, Z., Bohm, A., and Tang, W.J. (2002). Structural basis for the activation of anthrax adenylyl cyclase exotoxin by calmodulin. Nature *415*, 396-402.

Efthymiadis, A., Briggs, L.J., and Jans, D.A. (1998). The HIV-1 Tat nuclear localization sequence confers novel nuclear import properties. J Biol Chem *273*, 1623-1628.

Feng, C., Thomas, C., Holliday, M.A., Tollin, G., Salerno, J.C., Ghosh, D.K., and Enemark, J.H. (2006). Direct measurement by laser flash photolysis of intramolecular electron transfer in a two-domain construct of murine inducible nitric oxide synthase. J Am Chem Soc *128*, 3808-3811.

Fischer, R., Fotin-Mleczek, M., Hufnagel, H., and Brock, R. (2005). Break on through to the other side-biophysics and cell biology shed light on cell-penetrating peptides. Chembiochem *6*, 2126-2142.

Fonseca, S.B., Pereira, M.P., and Kelley, S.O. (2009). Recent advances in the use of cell-penetrating peptides for medical and biological applications. Adv Drug Deliv Rev *61*, 953-964.

Gachhui, R., Presta, A., Bentley, D.F., Abu-Soud, H.M., McArthur, R., Brudvig, G., Ghosh, D.K., and Stuehr, D.J. (1996). Characterization of the reductase domain of rat neuronal nitric

oxide synthase generated in the methylotrophic yeast Pichia pastoris. Calmodulin response is complete within the reductase domain itself. J Biol Chem *271*, 20594-20602.

Ghosh, D.K., and Salerno, J.C. (2003). Nitric oxide synthases: domain structure and alignment in enzyme function and control. Front Biosci *8*, d193-209.

Gifford, J.L., Walsh, M.P., and Vogel, H.J. (2007). Structures and metal-ion-binding properties of the Ca2+-binding helix-loop-helix EF-hand motifs. Biochem J *405*, 199-221.

Greif, D.M., Sacks, D.B., and Michel, T. (2004). Calmodulin phosphorylation and modulation of endothelial nitric oxide synthase catalysis. Proc Natl Acad Sci U S A *101*, 1165-1170.

Ikura, M., and Ames, J.B. (2006). Genetic polymorphism and protein conformational plasticity in the calmodulin superfamily: two ways to promote multifunctionality. Proc Natl Acad Sci U S A *103*, 1159-1164.

Johnson, C.K. (2006). Calmodulin, conformational states, and calcium signaling. A single-molecule perspective. Biochemistry *45*, 14233-14246.

Kubota, Y., Putkey, J.A., Shouval, H.Z., and Waxham, M.N. (2008). IQ-motif proteins influence intracellular free Ca2+ in hippocampal neurons through their interactions with calmodulin. J Neurophysiol *99*, 264-276.

Lee, W.S., Ngo-Anh, T.J., Bruening-Wright, A., Maylie, J., and Adelman, J.P. (2003). Small conductance Ca2+-activated K+ channels and calmodulin: cell surface expression and gating. J Biol Chem *278*, 25940-25946.

Maier, L.S., Ziolo, M.T., Bossuyt, J., Persechini, A., Mestril, R., and Bers, D.M. (2006). Dynamic changes in free Ca-calmodulin levels in adult cardiac myocytes. J Mol Cell Cardiol *41*, 451-458.

Martasek, P., Liu, Q., Liu, J., Roman, L.J., Gross, S.S., Sessa, W.C., and Masters, B.S. (1996). Characterization of bovine endothelial nitric oxide synthase expressed in E. coli. Biochem Biophys Res Commun *219*, 359-365.

Means, A.R., and Chafouleas, J.G. (1982). Regulation by and of calmodulin in mammalian cells. Cold Spring Harb Symp Quant Biol *46 Pt 2*, 903-908.

Mishra, O.P., Ashraf, Q.M., and Delivoria-Papadopoulos, M. (2009a). Mechanism of Increased Tyrosine (Tyr(99)) Phosphorylation of Calmodulin During Hypoxia in the Cerebral Cortex of Newborn Piglets: The Role of nNOS-Derived Nitric Oxide. Neurochem Res.

Mishra, O.P., Ashraf, Q.M., and Delivoria-Papadopoulos, M. (2009b). Tyrosine phosphorylation of neuronal nitric oxide synthase (nNOS) during hypoxia in the cerebral cortex of newborn piglets: the role of nitric oxide. Neurosci Lett *462*, 64-67.

Montgomery, H.J., Bartlett, R., Perdicakis, B., Jervis, E., Squier, T.C., and Guillemette, J.G. (2003). Activation of constitutive nitric oxide synthases by oxidized calmodulin mutants. Biochemistry *42*, 7759-7768.

Montgomery, H.J., Romanov, V., and Guillemette, J.G. (2000). Removal of a putative inhibitory element reduces the calcium-dependent calmodulin activation of neuronal nitric-oxide synthase. J Biol Chem *275*, 5052-5058.

Newman, E., Spratt, D.E., Mosher, J., Cheyne, B., Montgomery, H.J., Wilson, D.L., Weinberg, J.B., Smith, S.M., Salerno, J.C., Ghosh, D.K., and Guillemette, J.G. (2004). Differential activation of nitric-oxide synthase isozymes by calmodulin-troponin C chimeras. J Biol Chem *279*, 33547-33557.

Persechini, A., Blumenthal, D.K., Jarrett, H.W., Klee, C.B., Hardy, D.O., and Kretsinger, R.H. (1989). The effects of deletions in the central helix of calmodulin on enzyme activation and peptide binding. J Biol Chem *264*, 8052-8058.

Persechini, A., and Kretsinger, R.H. (1988). The central helix of calmodulin functions as a flexible tether. J Biol Chem *263*, 12175-12178.

Persechini, A., Kretsinger, R.H., and Davis, T.N. (1991). Calmodulins with deletions in the central helix functionally replace the native protein in yeast cells. Proc Natl Acad Sci U S A *88*, 449-452.

Persechini, A., and Stemmer, P.M. (2002). Calmodulin is a limiting factor in the cell. Trends Cardiovasc Med *12*, 32-37.

Putkey, J.A., Kleerekoper, Q., Gaertner, T.R., and Waxham, M.N. (2003). A new role for IQ motif proteins in regulating calmodulin function. J Biol Chem *278*, 49667-49670.

Putkey, J.A., Waxham, M.N., Gaertner, T.R., Brewer, K.J., Goldsmith, M., Kubota, Y., and Kleerekoper, Q.K. (2008). Acidic/IQ motif regulator of calmodulin. J Biol Chem *283*, 1401-1410.

Quadroni, M., James, P., and Carafoli, E. (1994). Isolation of phosphorylated calmodulin from rat liver and identification of the in vivo phosphorylation sites. J Biol Chem *269*, 16116-16122.

Quadroni, M., L'Hostis, E.L., Corti, C., Myagkikh, I., Durussel, I., Cox, J., James, P., and Carafoli, E. (1998). Phosphorylation of calmodulin alters its potency as an activator of target enzymes. Biochemistry *37*, 6523-6532.

Rashid, F., and Horobin, R.W. (1990). Interaction of molecular probes with living cells and tissues. Part 2. A structure-activity analysis of mitochondrial staining by cationic probes, and a discussion of the synergistic nature of image-based and biochemical approaches. Histochemistry *94*, 303-308.

Richard, J.P., Melikov, K., Vives, E., Ramos, C., Verbeure, B., Gait, M.J., Chernomordik, L.V., and Lebleu, B. (2003). Cell-penetrating peptides. A reevaluation of the mechanism of cellular uptake. J Biol Chem *278*, 585-590.

Roman, L.J., Sheta, E.A., Martasek, P., Gross, S.S., Liu, Q., and Masters, B.S. (1995). High-level expression of functional rat neuronal nitric oxide synthase in Escherichia coli. Proc Natl Acad Sci U S A *92*, 8428-8432.

Ruan, J., Xie, Q., Hutchinson, N., Cho, H., Wolfe, G.C., and Nathan, C. (1996). Inducible nitric oxide synthase requires both the canonical calmodulin-binding domain and additional sequences in order to bind calmodulin and produce nitric oxide in the absence of free Ca2+. J Biol Chem *271*, 22679-22686.

Said Hassane, F., Saleh, A.F., Abes, R., Gait, M.J., and Lebleu, B. (2009). Cell penetrating peptides: overview and applications to the delivery of oligonucleotides. Cell Mol Life Sci.

Slemmon, J.R., Morgan, J.I., Fullerton, S.M., Danho, W., Hilbush, B.S., and Wengenack, T.M. (1996). Camstatins are peptide antagonists of calmodulin based upon a conserved structural motif in PEP-19, neurogranin, and neuromodulin. J Biol Chem *271*, 15911-15917.

Spratt, D.E., Israel, O.K., Taiakina, V., and Guillemette, J.G. (2008). Regulation of mammalian nitric oxide synthases by electrostatic interactions in the linker region of calmodulin. Biochim Biophys Acta *1784*, 2065-2070.

Spratt, D.E., Newman, E., Mosher, J., Ghosh, D.K., Salerno, J.C., and Guillemette, J.G. (2006). Binding and activation of nitric oxide synthase isozymes by calmodulin EF hand pairs. Febs J *273*, 1759-1771.

Spratt, D.E., Taiakina, V., and Guillemette, J.G. (2007a). Calcium-deficient calmodulin binding and activation of neuronal and inducible nitric oxide synthases. Biochim Biophys Acta *1774*, 1351-1358.

Spratt, D.E., Taiakina, V., Palmer, M., and Guillemette, J.G. (2007b). Differential binding of calmodulin domains to constitutive and inducible nitric oxide synthase enzymes. Biochemistry *46*, 8288-8300.

Teruel, M.N., Blanpied, T.A., Shen, K., Augustine, G.J., and Meyer, T. (1999). A versatile microporation technique for the transfection of cultured CNS neurons. J Neurosci Methods *93*, 37-48.

Thorogate, R., and Torok, K. (2004). Ca2+-dependent and -independent mechanisms of calmodulin nuclear translocation. J Cell Sci *117*, 5923-5936.

Thorogate, R., and Torok, K. (2007). Role of Ca2+ activation and bilobal structure of calmodulin in nuclear and nucleolar localization. Biochem J *402*, 71-80.

Tilstra, J., Rehman, K.K., Hennon, T., Plevy, S.E., Clemens, P., and Robbins, P.D. (2007). Protein transduction: identification, characterization and optimization. Biochem Soc Trans *35*, 811-815.

Torok, K., Thorogate, R., and Howell, S. (2002). Studying the spatial distribution of Ca(2+)-binding proteins. How does it work for calmodulin? Methods Mol Biol *173*, 383-407.

Trehin, R., and Merkle, H.P. (2004). Chances and pitfalls of cell penetrating peptides for cellular drug delivery. Eur J Pharm Biopharm *58*, 209-223.

Venema, R.C., Sayegh, H.S., Kent, J.D., and Harrison, D.G. (1996). Identification, characterization, and comparison of the calmodulin-binding domains of the endothelial and inducible nitric oxide synthases. J Biol Chem *271*, 6435-6440.

Wadia, J.S., and Dowdy, S.F. (2005). Transmembrane delivery of protein and peptide drugs by TAT-mediated transduction in the treatment of cancer. Adv Drug Deliv Rev *57*, 579-596.

Wang, W., and Malcolm, B.A. (1999). Two-stage PCR protocol allowing introduction of multiple mutations, deletions and insertions using QuikChange Site-Directed Mutagenesis. Biotechniques *26*, 680-682.

Wu, B., Moulton, H.M., Iversen, P.L., Jiang, J., Li, J., Spurney, C.F., Sali, A., Guerron, A.D., Nagaraju, K., Doran, T., Lu, P., Xiao, X., and Lu, Q.L. (2008). Effective rescue of dystrophin improves cardiac function in dystrophin-deficient mice by a modified morpholino oligomer. Proc Natl Acad Sci U S A *105*, 14814-14819.

Yap, K.L., Kim, J., Truong, K., Sherman, M., Yuan, T., and Ikura, M. (2000). Calmodulin target database. J Struct Funct Genomics *1*, 8-14.

Zavortink, M., Welsh, M.J., and McIntosh, J.R. (1983). The distribution of calmodulin in living mitotic cells. Exp Cell Res *149*, 375-385.